Laboratory Evaluation of Static and Dynamic Sag in Oil-Based Drilling Fluids

Titus Ntow Ofei*, Norwegian University of Science and Technology; Dinesh Venkata Kalaga, City College of New York; Bjørnar Lund, SINTEF; Arild Saasen, University of Stavanger; Harald Linga, SINTEF; Sigbjørn Sangesland, Norwegian University of Science and Technology; Knud Richard Gyland, M-I SWACO, Schlumberger Norge AS; and Masahiro Kawaji, City College of New York

Summary

In this paper, we present the results of barite sag measurements before and after hot-rolled oil-based drilling fluids (OBDFs) using different approaches for characterization. We characterized the barite sag of a liquid column under static condition using light-scattering (LS) measurements, hydrostatic pressure measurements, and gamma densitometry. Under the dynamic condition, we used a rheometer with a grooved bob-in-cup measuring system to characterize barite sag in rotational and oscillatory shear conditions. Extensive rheological characterization of the drilling fluid samples, before hot rolling (BHR) and after hot rolling (AHR), is carried out. It is found that barite sag decreased in hot-rolled fluid samples from the LS, rotational, and oscillatory shear measurements. The rheological characterization of the fluid samples showed that heat-activated chemicals in the hot-rolled fluid sample increased the viscosity and elasticity, which contributed to lower barite sag and longer suspension of particles than BHR. Both hydrostatic and gamma densitometry measurements reveal more or less uniform compaction of barite particles in the fluid sample below the liquid layer. Time-dependent oscillatory shear measurements provide new insights on the structural character of drilling fluids to predict barite sag tendencies during the fluid design phase.

Introduction

Downhole pressure control is the major task of a drilling fluid. The drilling fluid can be water- or oil-based and is densified by addition of solid weight material particles. A successful drilling operation requires that the weight material is evenly dispersed in the drilling fluid during the entire drilling operation. Barite is the most common weight material. Hence, the tendency of weight material to separate out of the suspension is known as barite sag. Sag is a phenomenon directly resulting from physical properties of the weight material, such as size and weight of each particle combined with the number density of particles and the fluid microstructure affecting the rheological properties of the drilling fluid. The microstructure contributes to the viscous properties of the drilling fluid (Quemada 1998; Baldino et al. 2018), the gel formation properties, and the fluid's viscoelasticity. The particle settling and sag of weight materials in drilling fluids is a major concern when drilling and completing a well. Some of the problems associated with sag in the wellbore include pressure-control-related issues, fluctuation in torque and drag loads, difficulty in running of casing, displacement inefficiency during cementing operation, lost circulation, and stuck pipe, among others (Zamora and Jefferson 1994; Saasen et al. 1995; Skalle et al. 1999; Tehrani et al. 2004). Suspended weight material particles in drilling fluids in inclined wellbores tend to settle much more as a result of creating dynamic conditions by the sag itself, which may accelerate the sag process in a phenomenon called Boycott settling, after Boycott (1920), who observed the increased efficiency in separating red and white blood corpuscles when using skew test tubes. Other effects accelerating sag in inclined wellbore sections include pumping, tripping, or drillpipe rotation in which sag is more severe than in the static condition (Dye et al. 2001). An eccentric drillpipe induces more sag than a concentric one; however, pipe rotation has a greater impact on the reduction of sag in the eccentric case than in the concentric one as shown in detail by Nguyen et al. (2011, 2014).

Barite (BaSO₄), ilmenite (FeTiO₃), and hematite (Fe₂O₃) are some common minerals used as conventional weight materials in formulating drilling fluids. Among these weight materials, API-grade barite has remained the standard weight material in the drilling fluid industry. It is easily milled to a particle size that reduces the degree of settling and minimizes losses on shaker screens. Its inertness allows it to be used in a wide range of drilling fluids containing different chemical components (Tehrani et al. 2014). Because the mass densities of ilmenite (SG = 5.1) and hematite (SG = 4.7) are high compared with the commercial grade barite (SG = 4.2), they help to reduce the solid volume fraction in the drilling fluid, thereby lowering the impact of the weight materials on the fluid rheological properties. The accepted barite quality has changed recently. Currently, it is acceptable to have a barite density of approximate SG = 4.10 (Al-Bagoury and Steele 2012).

In the following, we will therefore use the term "barite sag" as a generic description of the settling of suspended weight material particles in drilling fluids. The sag tendency is also related to the particle number density. By reducing the number of particles, the interaction between the particles will be reduced, especially in low-to-medium drilling fluid density, and sag will be more severe. This effect of number density was calculated by Saasen et al. (1995), and it fits similar results in the food industry (Dickinson 1992). To mitigate this effect, other researchers, for example, Al-Bagoury and Steele (2012), developed micronized ilmenite blended with manganese tetra-oxide to create stable drilling fluids.

Field experiences along with laboratory studies have shown that OBDFs are more vulnerable for sag than water-based drilling fluids. Rules of thumb exist to minimize barite sag in field operations. It is often required not to dilute the drilling fluid with more than 5% premix per circulation with a pressure loss of 50 bar across the drill bit when drilling with OBDFs (Omland et al. 2007).

Barite sag is caused by settling of suspended barite particles, which can lead to variation in drilling fluid density. There are different techniques available in literature for detecting such particle sag in drilling fluids. Several methods ranging from the static test cell to standard viscometer to laboratory-scale flow loops are shown to be promising for detecting sag potential in drilling fluids (Omland et al. 2007). More advanced rheological methods have also been tested, and Saasen et al. (1995) found that by combining the linear viscoelastic (LVE) parameters G' and G'', a strong indication about a change in sag potential could be given.

This paper (SPE 199567) was accepted for presentation at the IADC/SPE International Drilling Conference and Exhibition, Galveston, Texas, USA, 3–5 March 2020, and revised for publication. Original manuscript received for review 25 May 2020. Revised manuscript received for review 23 July 2020. Paper peer approved 28 July 2020.

^{*}Corresponding author; email: titus.n.ofei@ntnu.no

¹SG = specific gravity = mass density divided by density of water

Copyright © 2020 Society of Petroleum Engineers

Using the static test cell method, the drilling fluid is poured into a tube or steel cell and then allowed to stay undisturbed for a specified amount of time. A sag factor is calculated as the ratio between the fluid density at the bottom of the test cell to the sum of fluid densities at the bottom and top of the test cell. A sag factor of 0.50 signifies that no sag has occurred, while a value greater than 0.52 indicates the occurrence of sag. It is noted, however, that this sag factor does not account for syneresis; that is, free liquid being allowed to create a seepage flow to the surface by partial agglomeration of particles (Bamberger et al. 1998; Omland et al. 2006).

Meanwhile, the viscometer sag test (VST) measurement technique was introduced by Jefferson (1991) for detecting sagging in dynamic condition. The VST consists of a regular rotational viscometer and thermocup where drilling fluid samples are heated in the thermocup to 49 or 66°C while shearing the drilling fluid at 100 rev/min for 30 minutes. A syringe is used to retrieve fluid samples from the bottom of the thermocup before and after testing, and then the samples are weighed on a sensitive balance. An increase in the fluid density indicates sagging. Despite the simplicity, direct measurement, and low cost of the VST, it lacks wide acceptance in the oilfield industry. To improve the reliability of the VST technique, Zamora and Bell (2004) introduced the viscometer sag shoe test measurement technique. An inclined sag shoe or thermoplastic shoe was incorporated into the VST to expedite barite settling and facilitate the gathering of the settled weight material particles into a collection well (Zamora 2011).

Laboratory scale flow loops have also been used to examine the sag potential in both static and dynamic conditions. A cylindrical sag testing cell was developed to measure the level of barite sag at static and dynamic conditions with shear rates from 0.0 to $0.82 \, \mathrm{s}^{-1}$ and temperatures of 27 (80) and 49°C (120°F) (Parvizinia et al. 2011). The authors mounted pressure sensors on the wall of the cylinder to measure sag tendencies of OBDF as a function of hydrostatic pressure gradient. It was concluded that high shear rates and elevated temperature resulted in significant barite sag. Saasen et al. (1995) used an inclined sag cell consisting of a 2.13-m long transparent pipe with inner diameter of 110 mm, tilted at 60° from vertical to correlate sag to rheological data under static and dynamic conditions. A concentric rod having an outer diameter of 25 mm was positioned along the axis of the pipe to provide reciprocating movement to simulate the movement of small diameter downhole hardware. The authors found that dynamic sag can be severe even when static sag is absent or relatively small and dynamic sag is partially related to low shear viscosity. Nguyen et al. (2011) conducted a dynamic barite sag study with OBDF using a rotational viscometer incorporated with sag shoe and a flow loop. The flow loop test section was 3.6 m (12 ft) long, consisting of a transparent outer casing with a 5 cm (2 in.) inner diameter and an inner drillpipe with a 2.5 cm (1 in.) outer diameter. The drillpipe could be rotated up to 200 rev/min with eccentricity changed from zero (concentric case) to unity (fully eccentric case). The authors concluded that the rotational viscometer when used to measure dynamic sag provided a conservative estimate and did not correlate with the flow loop sag tests. Meanwhile, with flow loop test, pipe rotation had a greater impact on reducing sag when the drillpipe is eccentric rather than concentric. An inclined sag tester of length 1.5 m fixed onto a vertical collector pipe was used by Skalle et al. (1999) to study the effect of rheological properties on particle settling and sag in both static and dynamic conditions. The difference in pressures between the bottom of the inclined pipe and the collector pipe determines whether the drilling fluid is stable or unstable. Dye et al. (2001) investigated the effect of shear rate on dynamic barite sag for invert-emulsion drilling fluids using a field viscometer capable of measuring at 0.0017 s⁻¹ and an eccentric wellbore-hydraulics flow loop of approximately 2 m in length. The study concluded that dynamic barite sag increased as hole angle increased from 45 to 60°, while the onset of dynamic sag occurred at shear rates less than 4 s⁻¹. A high-angle sag test device capable of detecting sag tendencies by the movement of the center of mass of the test fluid at temperatures up to 149°C (300°F) and deviation angle from 20 to 90° was designed by Jamison and Clements (1990). Their study concluded that viscosity parameters of drilling fluids, as measured with standard oilfield viscometers, are not fitted for predicting sag performance in extended reach drilling.

With the use of rheometers, attempts have been made to predict the stability of drilling fluids with respect to sag (Saasen et al. 1991; Ehrhorn and Saasen 1996; Maxey 2007). Marshall (2007) reported a laboratory study on OBDFs in which seven companies participated using their in-house instruments. The companies involved were Grace, Anton Paar, Brookfield, Malvern, OFITE, Baker Hughes, and Kelco oilfield group. Viscosity measurements of the base fluid indicated that there was broad agreement among the seven instruments, particularly at intermediate shear rates. Nonetheless, repeatability of the measurements revealed that only two instruments (Anton Paar and Malvern) produced values close to the theoretically expected results over a large range of shear rate. Ofei et al. (2019) examined the effects of shear rate and viscosity on dynamic barite sag of a field OBDF with an oil/water ratio (OWR) of 80:20 at 50°C using an Anton Paar (Ashland, Virginia, USA) rheometer MCR 302 and density meter DMA 5000. The dynamic sag was measured under steady and oscillatory, low-to-ultralow shear rates from 0.001 to 5.11 s⁻¹. They concluded that for higher viscosity, less-pronounced dynamic sag was observed, and the dynamic time sweep test gave a good indication of sag potential.

A few publications on experimental work on sedimentation in Newtonian and non-Newtonian fluids are also reviewed for completeness. Moreira et al. (2017) investigated the suspension sedimentation in Newtonian and non-Newtonian fluids using gamma densitometry. Their results indicated that settling behavior is different in Newtonian fluids and non-Newtonian fluids. The sedimentation rate was slower in Newtonian fluids when compared with the settling rate in shear-thinning fluids with the same apparent viscosity. Moreover, the time for complete settling in the thickened zone took a very long time.

Batch sedimentation of calcium carbonate particles (< 70-µm size) in drilling fluids was studied by Santos et al. (2018). They also performed rheological tests to understand the stability of drilling fluids. Gamma densitometry has been used to measure the local solid concentration in sedimentation zones. The settling velocity was determined in the free settling zone, assuming there is no wall effect. It is found that the settling rate is high in a nonthickened suspension zone compared with that in a thickened suspension zone. Rocha et al. (2020) have reported the settling of barite in paraffin-based synthetic drilling fluid. Gamma densitometry experiments were performed to measure the change in chordal averaged mud density at different column heights and time. They have developed a mathematical model based on the continuum mechanics for predicting the settling in all settling zones in batch sedimentation in synthetic drilling fluids. The settling process is characterized by three settling zones, namely, clear zone, free settling zone, and compression zone, and the authors found that the mathematical model predictions were in good agreement with the experimental data.

The present study, based on Ofei et al. (2020), addresses barite sag in OBDFs under the influence of static and dynamic conditions at ultralow to low shear rates. The issue of syneresis, which is the effect of colloidal material slightly grouping, thus leaving a flow path for the continuous material to flow up to the surface, is not discussed in this paper although the process is mentioned in one case. In this study, an approach to obtain static and dynamic barite sag measurements is presented to examine the effects of rheological and viscoelastic properties for typical field OBDFs on barite sag performance.

Materials and Methods

Fluid Components. The reference drilling fluid is a common OBDF with an OWR of 80:20 and density of 1430 kg/m 3 (SG = 1.43). The fluid components were supplied by M-I Swaco, Schlumberger in Norway, and consisted of a refined mineral oil as a base fluid of density 814 kg/m 3 and kinematic viscosity of 5.9 mm 2 /s, brine of calcium chloride, lime, emulsifier, organophilic clay viscosifiers,

fluid-loss agent, low-gravity calcium carbonate, and API-grade barite. A spindle mixer was used to mix the components of the drilling fluid at a speed of 6,000 rev/min for a total of 70 minutes. **Table 1** shows the various components of the drilling fluid, including their mass fraction, concentration, and mixing time. The experiments reported here have been conducted in two different laboratories using the same drilling fluid. The drilling fluid was prepared in the respective laboratories using the same recipes and mixing protocols, with the same components from the same supplier.

Mixing Order	Product	Mass Fraction	Concentration (g/L)	Mixing Time (minutes)
1	Refined mineral oil (base fluid)	0.35	501.9	_
2	Emulsifier	0.0139	20.0	2
3	Viscosifier (low-temp. clay)	0.00628	9.0	4
4	Viscosifier (high-temp. clay)	0.00907	13.0	4
5	Lime	0.0139	20.0	5
6	Fluid-loss agent	0.00697	10.0	5
7	Calcium chloride brine	0.139	199.3	15
8	API barite (weight material)	0.426	610.8	25
9	Calcium carbonate (low gravity)	0.0349	50.0	10

Table 1—Components of 1 L of SG = 1.43 OBDF.

Particle-Size Distribution (PSD). The particle sizes of API barite for SG in the range of 4.1 to 4.2 were characterized using an LS particle-size analyzer. The instrument uses laser light with a wavelength of 750 nm to size particles with diameters from 0.04 to 2000 μ m by light diffraction. The laser's radiation passes through a spatial filter and projection lens to form a beam of light. The beam passes through the sample cell where particles suspended in liquid or air scatter the incident light in characteristic patterns, which depends on their sizes (Beckman Coulter, Inc. 2011). **Fig. 1** shows the PSD of the API barite with D_{10} , D_{50} , and D_{90} values as 0.658, 6.909, and 34.130 μ m, respectively. The D_x value indicates that x% of the particles by mass have diameters that are smaller than this value.

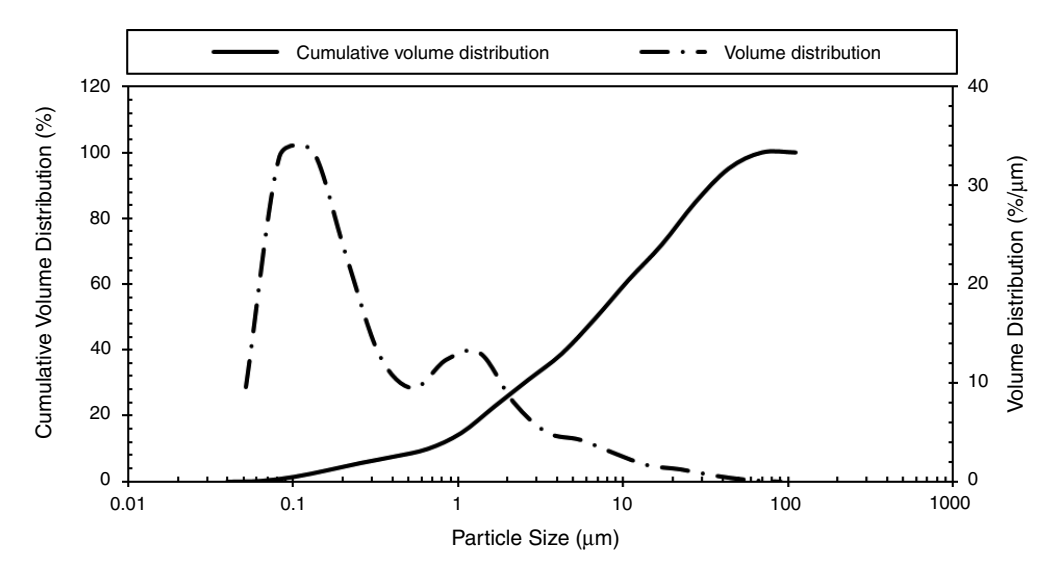


Fig. 1—PSD of API barite.

Fluid Mixing Procedure. In preparation of the drilling fluid, the following procedure was used for mixing. The drilling fluid components, concentration, and mixing procedure were recommended by the supplier:

- 1. Pour the refined mineral oil in a container and place the container in an ice water bath to maintain the fluid's temperature below 65°C. The use of a cooling bath is not necessary until the temperature exceeds 55°C. It should be noted that some of the components require initial heating to better dissolve in the base oil and to be fully activated.
- 2. Pour the base oil into a spindle mixer container, add the emulsifier, and mix for 2 minutes.
- 3. Add the low-temperature and high-temperature viscosifiers to the mixing container and mix for 4 minutes apart.
- 4. Afterward, add the lime to the container and mix for 5 minutes.
- 5. Add the fluid-loss agent and mix for 5 minutes.
- 6. Add the brine of calcium chloride and mix for 15 minutes.
- 7. Add the barite and mix for 25 minutes.
- 8. Finally, add the calcium carbonate to the mixture and mix for 10 minutes to act as a bridging material, which reduces fluid loss and minimizes filter-cake thickness, especially in permeable formation.

The final SG of the drilling fluid sample was measured to be 1.43. Two sets of fluid samples of the same compositions were mixed in which one was preconditioned at atmospheric temperature and pressure and the other was transferred into an aging cell, pressurized at 6.8 bar (100 psi) using nitrogen gas, and hot-rolled at 120°C for 60 hours using an OFITE 172-00-1-C roller oven with programmable timer and circulating fan. An emulsion stability tester, which applies a precision voltage-ramped sinusoidal signal across a pair of parallel flat-plate electrodes was used to determine the fluid's electric stability. A pH meter was used to measure the concentration of hydrogen ions in the drilling fluid samples. The electrical stability and pH readings of the sample preconditioned at atmospheric pressure were recorded as 922 V and 10.35, respectively. Furthermore, the recorded electric stability and pH values of the sample AHR were 684 V and 9.92, respectively.

Characterization of Barite Sag in Static and Sheared Fluids. We have used four different approaches for characterizing barite sag.

- Light transmission and backscattering (static fluids)
- Rheological and density measurement using rotational rheometer and densitometer (sheared fluids)
- Hydrostatic pressure gradient (static fluid)
- Gamma densitometry (static and sheared fluid)

Characterization Using Optical Stability Analyzer. The stability of the dispersed API barite particles in the OBDF at static condition was evaluated using an optical stability analyzer, specifically, Turbiscan® Lab Expert analyzer (Formulaction 2008). The principle of this instrument is based on static multiple LS using a monochromatic infrared light source of wavelength, $\lambda = 880$ nm, and two synchronous detectors: a transmission detector that receives the light going across the sample at 0° from the incident beam and a backscattering detector that receives the light scattered backward by the sample at 135° from the incident beam (Liu et al. 2014). The detection head scans the entire length of the sample acquiring transmission and backscattering data every 40 μ m. The stability analyzer can be thermoregulated from 5 to 60°C for a long-term stability analysis. The obtained curves of backscattering as a function of the height of the sample reflect the microscopic characteristics of growth or migration of particles at a given time (Lu et al. 2017). The instrument can handle a wide range of particle sizes from 10 nm to 1000 μ m and particle concentration from 10⁻⁴ to 95%. Fig. 2 shows a schematic of the stability analyzer.

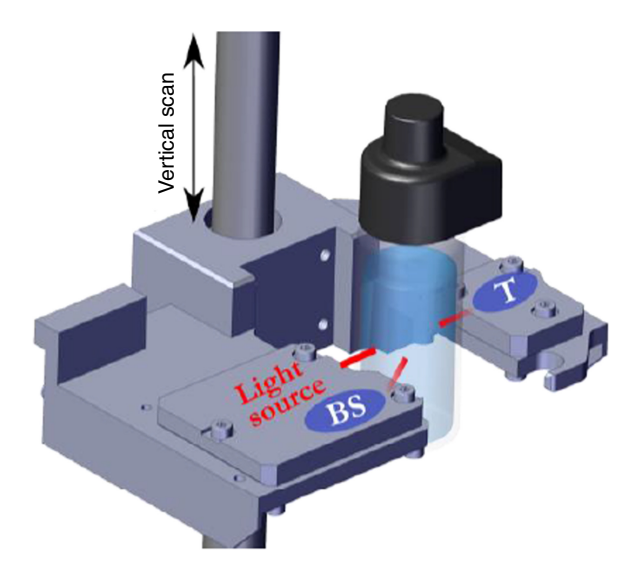


Fig. 2—Schematic of the stability analyzer (T = light transmission; BS = backscattering).

The stability analyzer scans at various preprogrammed times and overlays the signals on one graph to show the destabilization phenomenon. Graphs are usually displayed in reference mode, whereby the first signal profile is subtracted from all other profiles to enhance variations. Destabilization phenomena such as sedimentation, flocculation, coalescence, and creaming of the colloidal system can be interpreted from the change in backscattering (Δ BS) signals. Sedimentation has occured when Δ BS signals peak up at the bottom of the sample and peak down at the top of the sample. A reverse in the peaks, however, describes a creaming phenomenon. If there is a variation in the Δ BS signals recorded in the middle part of the sample, this indicates flocculation or coalescence due to the variation in particle size.

A fingerprint spectrum that can characterize the dispersion property of the drilling fluid samples was measured by setting the measurement frequency, scanning time, and scanning interval. In this study, a 20 cm³ fluid sample each, BHR and AHR, was filled into a cylindrical glass tube of height 55 mm and placed in the stability analyzer. The two optical sensors were used to scan along the height of different samples sealed in the glass tube. A total of a 7-day scanning period was set at a frequency of one scan per hour. All scans were conducted at 25°C. The stability of the fluid samples was characterized by the so-called Turbiscan Stability Index (TSI) with the help of a software. The TSI is the sum of all the backscattering and transmission variations over the entire height of the sample. The more the Turbiscan signal evolves, the higher the TSI. Therefore, a high TSI value corresponds to an unstable fluid sample. The TSI is calculated as (Yang et al. 2017):

$$TSI = \sqrt{\frac{\sum_{i=1}^{n} (x_i - x_{bs})^2}{n-1}}, \qquad (1)$$

where n is the number of scan times, x_i is the backscattering light intensity at the scanning time of i, and x_{bs} is the average backscattering light intensity. The computed TSI takes into account all the destabilization phenomena occurring in the sample, including any eventual bubbles and syneresis, as well as the size variation. The TSI is characterized based on five different scales deduced from empirical

analysis of a database of more than 500 measurements (Formulaction 2008). The definitions of the scales are as follows: "A + = 0.0 - 0.5", no significant destabilization; "A = 0.5 - 1.0", emerging destabilization; "B = 1.0 - 3.0", weak destabilization; "C = 3.0 - 10.0", significant destabilization; and " $D \ge 10.0$ ", high destabilization.

According to a general law of sedimentation, the particle migration (settling) rate can be defined by Stokes' law extended to concentrated dispersions following the definition by Mill and Snabre (1994):

$$V(\phi, d) = \frac{gd^2(\rho_p - \rho_f)}{18\eta} \frac{(1 - \phi)}{\left[1 + \frac{4.6\phi}{(1 - \phi)^3}\right]}, \qquad (2)$$

where ϕ is the particle concentration (-), d is the particle mean diameter (m), g is acceleration of gravity (m/s^2), ρ_p is particle density (kg/m^3), ρ_f is continuous phase density (kg/m^3), and η is the continuous phase dynamic viscosity (Pa·s). This formula is valid for

Newtonian fluids in the Stokes flow regime (i.e., particle Reynolds number much smaller than unity) with $\phi < \frac{4}{7}$, which corresponds to random isostatic packing before restructuring (Dixmier 1978). A stability analyzer software, Turbiscan LAB (Formulaction, Toulouse, France), uses Eq. 2 to compute the migration rate by monitoring the speed of formation of particle layers and characterizing the motion of the particles.

Characterization Using Rotational Rheometry. An Anton Paar rheometer (MCR 302) using a Couette geometry with a grooved bob was used to conduct the rheological measurements on the OBDF at 25°C. The various rheological tests performed include flow curves, oscillatory amplitude sweep, oscillatory frequency sweep, and tests at constant rotational and oscillatory shear rates.

The flow curves were measured under controlled shear rates and show the shear stress vs. shear rate of the sample. We presheared the sample at a constant shear rate of $1022 \, \mathrm{s}^{-1}$ for 300 seconds before linearly ramping down the shear rate from $1022 \, \mathrm{to} \, 1.0 \, \mathrm{s}^{-1}$ for $100 \, \mathrm{measuring}$ points with a 5-second measuring duration per point. Then, the shear rate was logarithmically ramped down from $1.0 \, \mathrm{to} \, 0.001 \, \mathrm{s}^{-1}$ for 40 measuring points with a 4-second measuring duration per point to capture the flow characteristics in the ultralow shear-rate region. In a similar manner, the shear rate was ramped up logarithmically from $0.001 \, \mathrm{to} \, 1.0 \, \mathrm{s}^{-1}$ for 40 measuring points with 4-second measuring point duration and then linearly ramped up from $1.0 \, \mathrm{to} \, 1022 \, \mathrm{s}^{-1}$ for a total of $100 \, \mathrm{measuring}$ points with 5-second measuring point duration. A difference between the ramping down and ramping up flow curves indicates the thixotropy of the fluid sample (Jachnik 2005; Cayeux 2020). In this present study, we reveal insignificant differences between the flow curves.

The amplitude sweep tests that use sinusoidal oscillations allow the testing of the microstructure of the sample without breaking the sample structure (Savari et al. 2013). The test was carried out with a constant angular frequency of 10 rad/s and increasing strain amplitude from 0.001 to 100% at a slope of 5 measuring points per decimal, accounting to 26 measuring points. The limit of the LVE range, below which the measured properties of the sample are nondestructive, is determined for use as a parameter for the frequency sweep test at a tolerance limit of 97%. The test also measures the storage modulus (G'), characterizing the material's elastic behavior, and loss modulus (G''), characterizing the viscous behavior of the material. The flow point, where G' = G'', is measured as the point where the material's microstructure deforms and initiates flow. If G' > G'', the elastic behavior dominates the viscous behavior, and the sample depicts a solid-like character. Conversely, G'' > G', indicates that the viscous behavior dominates the elastic behavior of the sample and shows a liquid-like character.

By performing oscillatory shear tests, certain parameters have been adopted from continuum mechanics to measure the rheological properties of the viscoelastic fluid. The shear modulus G, under uniaxial stress conditions, according to Hooke's law, is constant for perfectly elastic material. However, for oscillatory stresses, a complex shear modulus, G^* , which is divided into a storage modulus, G', and a loss modulus, G'', is defined by the following equations (Mezger 2014):

$$G^* = \frac{\tau_A}{\gamma_A} \,, \qquad \dots \tag{3}$$

$$G' = |G^*|\cos(\delta) = \left|\frac{\tau_A}{\gamma_A}\right|\cos(\delta), \qquad (4)$$

$$G'' = |G^*|\sin(\delta) = \left|\frac{\tau_A}{\gamma_A}\right|\sin(\delta), \qquad (5)$$

where τ_A is the complex stress amplitude, γ_A is the corresponding complex strain amplitude, and δ is the phase shift angle between τ_A and γ_A .

The frequency sweep test uses sinusoidal oscillations at small strain amplitudes usually within the LVE range (Savari et al. 2013). A shear strain amplitude within the LVE range was applied on the sample over a decreasing range of angular frequency from 100 to 0.001 rad/s at a slope of 5 measuring points per decimal. A comparison of G' and G'' is of greater importance at lower frequencies in which dynamic sag is more likely to occur. From G' and G'', we can calculate the phase shift angle δ , which is also called the damping

factor of the sample and defined as $\tan(\delta) = \frac{G''}{G'}$. The phase shift angle and the damping factor characterize the viscoelastic behavior of the sample, where $\delta = 0^{\circ}$ corresponds to ideal elastic solid behavior, and $\delta = 90^{\circ}$ corresponds to purely viscous liquid behavior. Thus, the sample is more viscous when $\tan(\delta) > 1$, and more elastic when $\tan(\delta) < 1$ (Tehrani et al. 2004).

During the steady-state test, the viscosity of the sample was measured at a constant shear rate in isothermal condition (25°C) for a fixed length of time. The constant shear rates used were 10.22, 5.11, 1.7, 0.60, 0.10, 0.01, and 0.001 s^{-1} . The duration and the number of measurement points were 10,800 seconds and 1,000, respectively, per shear rate. A total of 14 test runs were carried out for the constant rotational time test.

For the time-dependent oscillatory test, both strain amplitude and angular frequency were held constant. Angular frequencies from 10.22 to 0.001 rad/s and strain amplitudes of 0.05 and 100% were imposed. The strain amplitude of 0.05% is a value within the LVE range in which the microstructure of the fluid sample remains undisturbed, whereas 100% strain amplitude was imposed to simulate high vibration effect of the drillstring. Each experiment was run for a total time of 10,800 seconds at 1,000 measuring points with a 4-second interval. An isothermal condition of 25°C was imposed, and a total of 21 test runs were carried out.

Dynamic Sag Testing. The testing of the dynamic barite sag of the fluid samples was performed using a combination of a controlled shear rate rheometer and accurate density measurements as shown in Fig. 3. The rheometer had a Couette geometry in which the inner cylinder (the grooved bob) rotated while the outer cylinder (the cup) was fixed. The rotational velocity is limited by a specified input torque; that is, the shear stress of the bob continuously changes to produce the torque limit set by the instrument (Saasen et al. 1991). Two time-dependent conditions were separately imposed on the rheometer, which were constant rotational and oscillatory sweep. A digital density meter with an uncertainty of $\pm 5 \times 10^{-5}$ g/cm³ was used to measure the density of the fluid samples. It is based on a U-tube principle, which measures the inertial mass of a known sample volume. The fluid sample is filled into a U-shaped tube that is mounted on a countermass using a syringe. The U-tube is then excited and the fluid starts to oscillate. The change in frequency is then measured, and the density can be determined (Hold 2015). The instrument performs several measurements automatically.

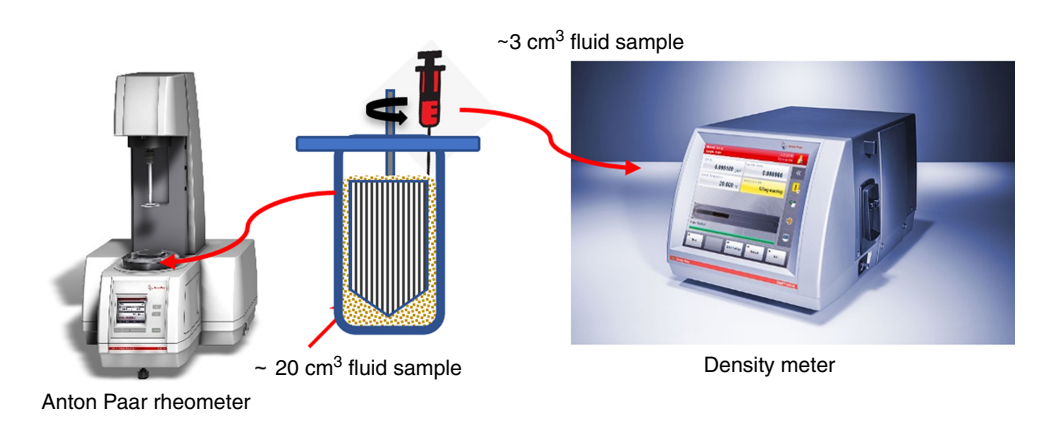


Fig. 3—Experimental setup for dynamic sag measurement.

To conduct the dynamic sag test, we first presheared the fluid samples for 2 minutes using the spindle mixer, took approximately 3 cm³ of the fluid sample in a syringe, and injected it into the digital density meter and measured the initial density ρ_{initial} at 25°C. Next, approximately 20 cm³ of the fluid sample was filled into the rheometer measuring cup, and a constant shear rate or constant frequency (0.001 to 1022 s⁻¹) was imposed and run for 10,800 seconds (3 hours) at 25°C. After each run, a syringe was used to draw approximately 3 cm³ of the fluid sample from the top of the measuring cup and injected into the digital density meter for the final density ρ_{final} to be measured. If the measured fluid sample's final density is less than the initial density, sag has occurred. The dynamic sag density $\Delta \rho$ and dynamic sag index (DSI) are respectively calculated using Eqs. 6 and 7. For a fluid to exhibit perfect suspension characteristics, the DSI should be 0.50. A fluid that has a DSI greater than 0.53 is considered to have inadequate suspension properties (Maxey 2007). It should be noted that for a single fluid sample injection into the density meter, three series of measurements were taken, after which the average value of these measurements were calculated.

$$\Delta \rho = \rho_{\text{initial}} - \rho_{\text{final}}, \qquad (6)$$

$$\Delta \rho = \rho_{\text{initial}} - \rho_{\text{final}}, \qquad (6)$$

$$DSI = \frac{\rho_{\text{initial}}}{2\rho_{\text{final}}}. \qquad (7)$$

Important parameters such as dynamic viscosity and complex viscosity were also measured and examined. The complex viscosity η^* , which defines the viscoelastic flow resistance of the sample, is expressed as (Mezger 2014):

$$\eta^* = \frac{\tau(t)}{\dot{\gamma}(t)}, \qquad (8)$$

where $\tau(t)$ and $\dot{\gamma}(t)$ are the complex stress and shear rate, respectively.

Characterization Using Hydrostatic Pressure and Gamma Densitometry Measurements. Particle sedimentation in general and barite sag in particular can also be studied in columns of fluid by measuring the transient hydrostatic pressure gradients across a vertical distance. From this, the average particle volume fraction in the corresponding volume of fluid can be determined, which can also be determined by measuring the attenuation of a beam of gamma radiation. We here demonstrate the use of these methods to study barite sedimentation in water.

Experiments for static flow conditions were conducted in a cylindrical acrylic column with a 5.7 cm internal diameter and 70 cm height. The setup also includes two individual data acquisition units, pressure transducers (PTs), a pair of gamma radiation source and detector, and a computer.

Fig. 4 shows a schematic of the static cell equipped with PTs (Omega: PX309), a gamma source, and 2-in. detector (Canberra Inc., Meriden, Connecticut, USA). Four PTs were flush mounted on the outer cylinder at different heights 2.4, 9.8, 31.8, and 46.7 cm from the bottom. Before the actual experiment, barite and water were well mixed at 6,000 rev/min for 10 minutes using a high shear homogenizer (Silverson: L-5MA). The well-mixed water and barite mixture were then transferred to the Taylor-Couette cell, and air bubbles were injected through the bottom of the test cell to avoid settling of the barite before the sag tests. After achieving a uniform distribution of barite in the column, air injection was stopped, and the hydrostatic pressure and gamma densitometry measurements were started simultaneously. The hydrostatic pressure gradient was calculated from the instantaneous pressure/time data series, and the data were used to calculate the solid mass fraction using Eq. 9:

$$\phi_s = \frac{(\Delta P_M - \Delta P_L)}{(\Delta P_S - \Delta P_L)}, \qquad (9)$$

where ϕ_s is the volume fraction of solid particles, ΔP_M is the measured hydrostatic pressure, ΔP_L is hydrostatic pressure from a solidsfree liquid, and ΔP_S is the weight of solid particles per unit area of a column given by,

$$\Delta P_s = g\rho_s(h_2 - h_1). \qquad (10)$$

$$\rho_m = \rho_l(1 - \phi_s) + \rho_s\phi_s. \qquad (11)$$

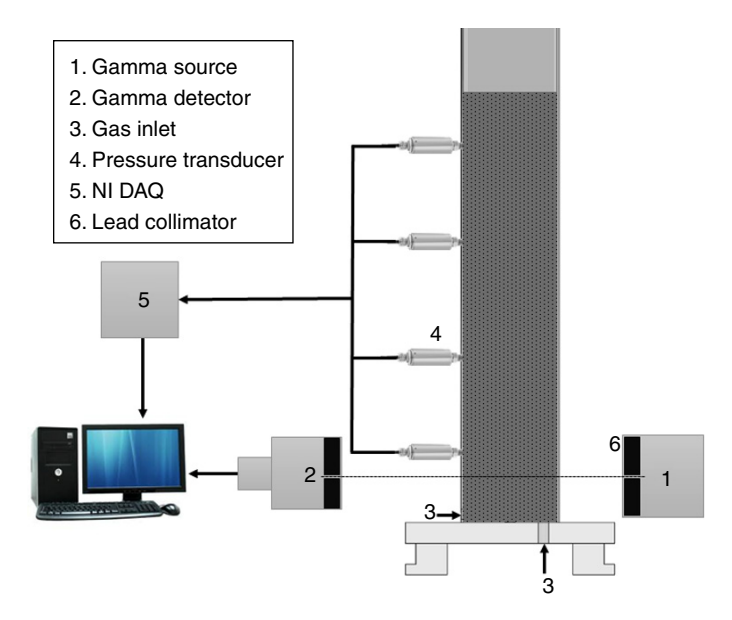


Fig. 4—Schematic of the static cell test facility with National Instrument Data Acquisition (NI DAQ) used in the present work.

A 5 mCi Cesium-137 isotope was used as a gamma source, and a 5-cm diameter NaI scintillation detector was used to measure the transmitted gamma radiation. Collimators made of 5-cm thick lead plates were placed on both the detector and source sides to create a 3-mm pencil beam (Fig. 4). The gamma beam scans were performed at an elevation of 5 cm from the bottom of the static cell. The change in counts with time were recorded and used to calculate the fluid density using the Beer–Lambert law:

$$I = I_0 e^{-\alpha L}, \qquad (12)$$

where I is the gamma beam intensity after passing through a medium with a linear attenuation coefficient α , I_0 is the incident intensity of the gamma beam, and L is the path length of the gamma beam through the medium.

For a liquid/solid mixture, we have

$$I_m = I_0 \exp\{-\left[\alpha_l(1-\phi_s) + \alpha_s\phi_s\right]L\}, \qquad (13)$$

where α_l and α_s are the linear attenuation coefficients of liquid and solid particles, respectively.

The volume fraction of solids ϕ_s can be found by measuring the intensity I_l with the pure liquid (without solid particles), the corresponding intensity I_b with a fully sedimented bed with a known volume fraction ϕ_b of solids, and the intensity I_m with the liquid/solid mixture, as given by

$$\phi_s = \phi_b \frac{ln\left(\frac{I_m}{I_l}\right)}{ln\left(\frac{I_b}{I_l}\right)} . (14)$$

Gravitational settling experiments in static cell with three different initial barite weight fractions were performed. Fig. 5 shows the change in the solid fraction with respect to the time for three initial barite concentrations in a static cell. Because the void fraction was calculated from the hydrostatic pressure obtained from the top PT pair, the data in Fig. 5 indicates the drop in the solid fraction as the particles settle from the top measurement region. Hence, the hydrostatic pressure data recorded by the top PT pair is related to the free settling velocity of the barite. It is found from the data that initial settling velocity in the static cell is 0.1 mm/s and hindered settling velocity is 0.03 mm/s, approximately. The settling velocity for the isolated sphere can be calculated from Stokes' law, using Eq. 15:

$$v_s = \frac{2\Delta\rho g a^2}{9\mu(\hat{\gamma}_{\text{eff}})}, \qquad (15)$$

where $\Delta \rho = \rho_p - \rho_f$ is the density difference between barite and water, a is the particle radius, and μ is the fluid effective viscosity at a representative shear rate.

$$\dot{\gamma}_{\text{eff}} = \frac{v_s}{a}.$$
 (16)

The hindered settling velocity v_{sh} for an ensemble of particles of identical size can be expressed as

$$v_{sh} = v_s H(\phi)$$
. (17)

The hindered settling function $H(\phi)$ has been used to calculate the hindered settling velocity v_{sh} .

$$H(\phi) = (1 - \phi)^m, \quad \dots \tag{18}$$

where m=4.48 for non-Brownian systems. The experimental hindered settling value is very similar to the hindered settling velocity derived from Stokes' law with a hindered settling factor $f(\phi)$ for a mean particle diameter of 30 μ m. The calculated hindered settling velocity is 0.03 mm/s.

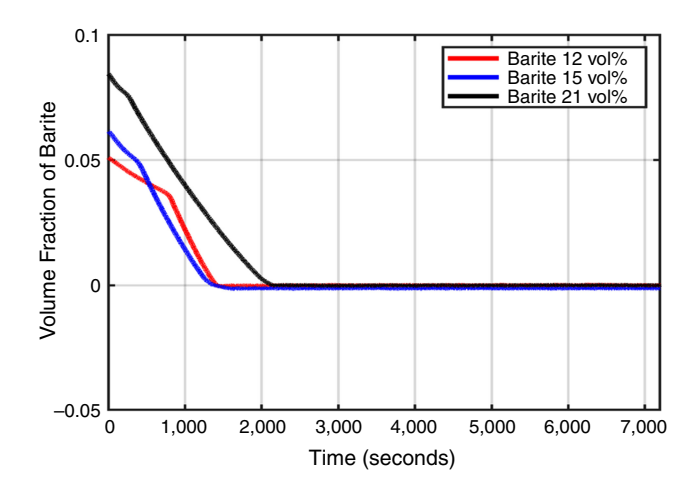


Fig. 5—Variation of solid fraction with time for the top PT pair.

For the gamma densitometer measurements, the number of photons detected over a counting period of 8 minutes was recorded, and the gamma measurements were made at the bottom of the test section. The gamma counts recorded by the detector were normalized by the initial counts at t = 0 for the three initial barite concentrations as shown in **Fig. 6a.** The gamma counts decreased with time due to greater attenuation of gamma rays caused by the increased concentration of barite particles at the bottom of the cell. The rate of barite sedimentation is seen to be slower for the higher initial barite concentration because higher particle number density causes hindered settling and reductions in the settling velocity. Fig. 6b shows the changes in the volume-averaged solid fraction (pressure difference method) and chordal-averaged solid fraction (gamma densitometry method) with time for all three initial barite concentrations. The pressure difference was obtained from the bottom PT pair, and a gamma scan was also performed at the bottom (Fig. 4). The two methods show good overall consistency with each other. There is a deviation between the two methods at later times and at the highest barite volume fractions. As the solids fraction increases, particle-particle interactions become more important and carry an increasing fraction of the particle weight. This is not accounted for in the model presented in Eq. (9). The gamma measurements (Fig. 6a) show that a steady state has not yet been reached (between t = 2,000 and 7,000 seconds), indicating an ongoing compaction. In this regime, the pressure method is not valid. This method should therefore be used with caution.

It is evident from Fig. 6b that the chordal average solid fractions and volume-average solid fractions of barite start increasing immediately at t = 0, increase steadily during the first 1,300 seconds and then more slowly (gamma method, see also Fig. 6a) or become steady (pressure method) after approximately 2,000 seconds. Note also from Figs. 6a and 6b that the gamma method shows increasing local solid fraction for higher initial barite particle concentration, even for the later part of the experiment.

Analysis on Rheological and Viscoelastic Properties

Flow and Viscosity Curves. The shear stress and viscosity flow curves of the fluid samples for both BHR and AHR are presented in Figs. 7 and 8, respectively. The shear stress vs. shear rate relationship describes a pseudoplastic shear-thinning behavior of the drilling fluid samples as shown in Fig. 7. Below the shear rate of $0.1 \, \text{s}^{-1}$, the percentage difference between the shear stress values of both fluid samples ranged from 50 to 93%. The percentage difference decreased between 0.1 and $100 \, \text{s}^{-1}$, after which it remained almost constant at 10% from 100 to $1022 \, \text{s}^{-1}$. The viscosity profiles of the drilling fluid samples decreased monotonously with increasing shear rate with a slightly higher viscosity for the hot-rolled fluid sample as presented in Fig. 8. The curve is linear between 0.1 and $1.0 \, \text{s}^{-1}$, indicating a power-law region, whereas a gradual transition toward a quasi-Newtonian region exists between 10 and $1022 \, \text{s}^{-1}$. The hot-rolled fluid sample shows a slightly higher viscosity. The reason for the increase in viscosity is likely that the viscosifiers are activated by the heating process.

Amplitude Sweep. Fig. 9 shows the amplitude sweep curves of the drilling fluid samples, which describe the dependence of the loss modulus G'' and storage modulus G' on oscillation amplitude. The limit of the LVE range, which was measured at a tolerance limit of 97%, occurs at a shear strain of 0.10% for both fluid samples. Within the LVE range, the microstructure of the fluid sample remains undisturbed. However, beyond the LVE range, both G' and G'' curves drop continuously, thus indicating a gradual breakdown of the superstructure of the fluid sample. The flow point where G' = G'' occurs at a shear strain and G' of 24.3% and 5.4 Pa, respectively, for the BHR sample. Similarly, the flow point for the AHR sample occurred at a shear strain and G' of 24.4% and 10.2 Pa, respectively. Beyond the flow point, the fluid sample becomes predominantly viscous liquid. Both viscous and elastic properties of the fluid sample increased in the AHR sample compared with the BHR sample by nearly a factor of 2 and 2.5 for G' and G'', respectively, at the limit of LVE. Within the limits of LVE range, both fluid samples are predominantly elastic, which indicates their yield stress ability. At very low shear rates, Brownian motion will maintain the small barite particles and water droplets in its local volume location. For a certain strain, these droplets and particles need to leap-frog to allow for flow. At this point, the yield stress is anticipated to be overcome. The dynamic yield stress refers to a quantity measured under dynamic conditions at which a constant or time-varying shear rate is applied and can be measured more accurately from the amplitude sweep from which the yield stress of the material is determined as the shear stress where $G' = 0.9G'_{lin}$. So long as the stresses below the yield stress are applied, no significant change of the internal structure could

occur; hence, the sample would show reversible viscoelastic behavior. A higher yield stress fluid indicates a high suspension capability of the fluid sample. From Fig. 9, the yield stress values predicted for BHR and AHR fluid samples are 0.40 and 0.936 Pa, respectively. It should be noted that the yield stress predicted from the amplitude sweep could be slightly different from the yield stress predicted using the flow curve because the amplitude sweep test was performed with a constant angular frequency of 10 rad/s.

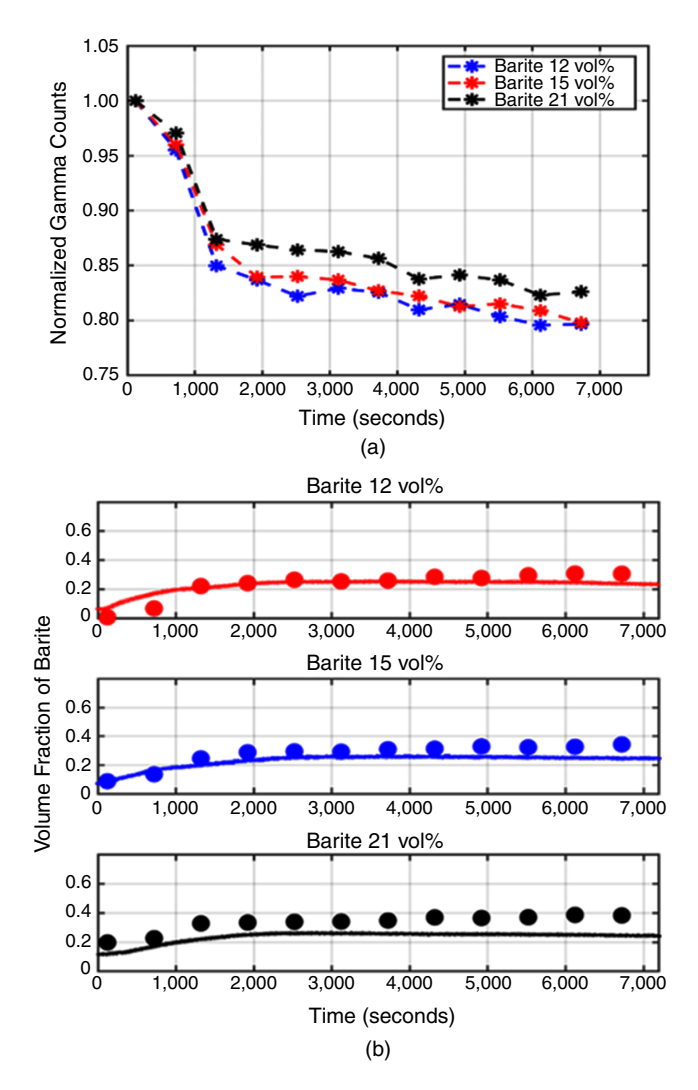


Fig. 6—(a) Variations of normalized gamma counts with time and (b) comparison of solid fraction values for all three initial barite concentrations measured using gamma densitometry (solid dots) and pressure difference methods (solid lines).

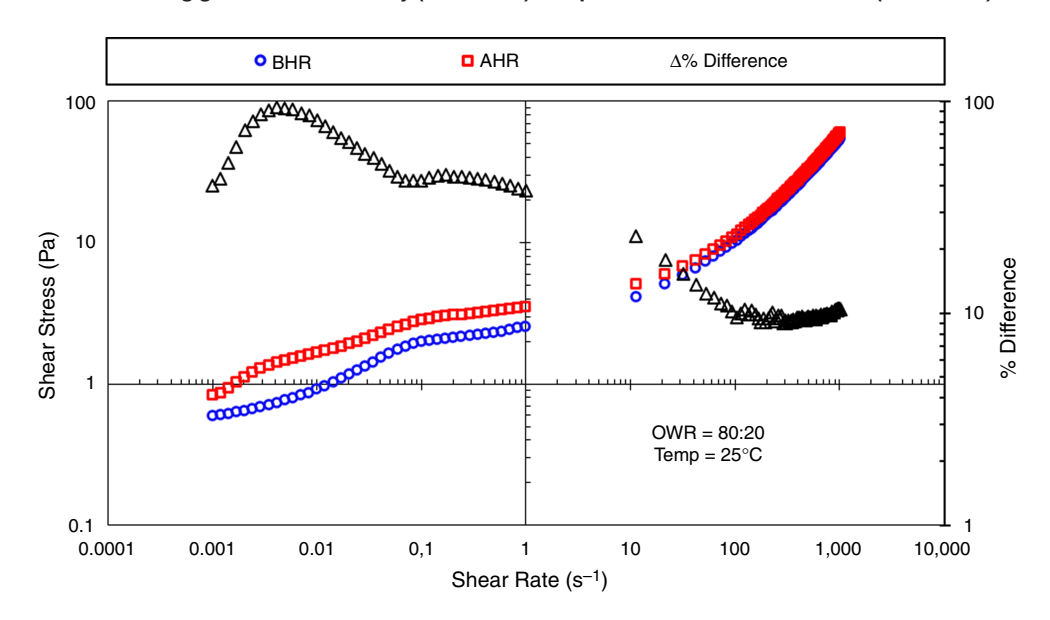


Fig. 7—Flow characteristic curves between BHR and AHR drilling fluid samples with the OWR of 80:20 measured at 25°C. The AHR sample was measured after dynamic aging in a roller oven at 120°C for 60 hours.

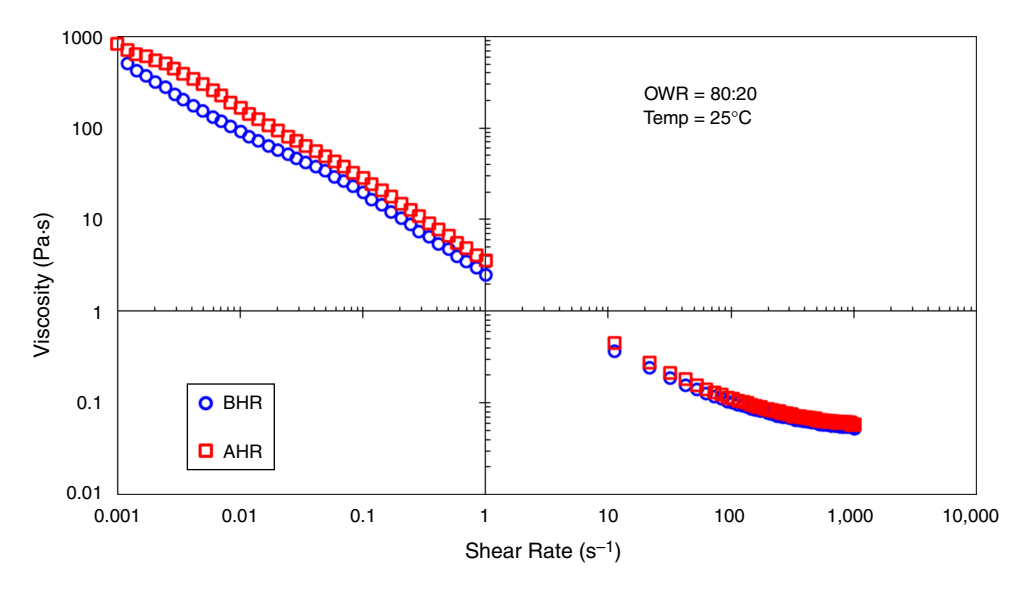


Fig. 8—Viscosity profiles between BHR and AHR drilling fluid samples with OWR of 80:20 measured at 25°C. The AHR sample was measured after dynamic aging in a roller oven at 120°C for 60 hours.

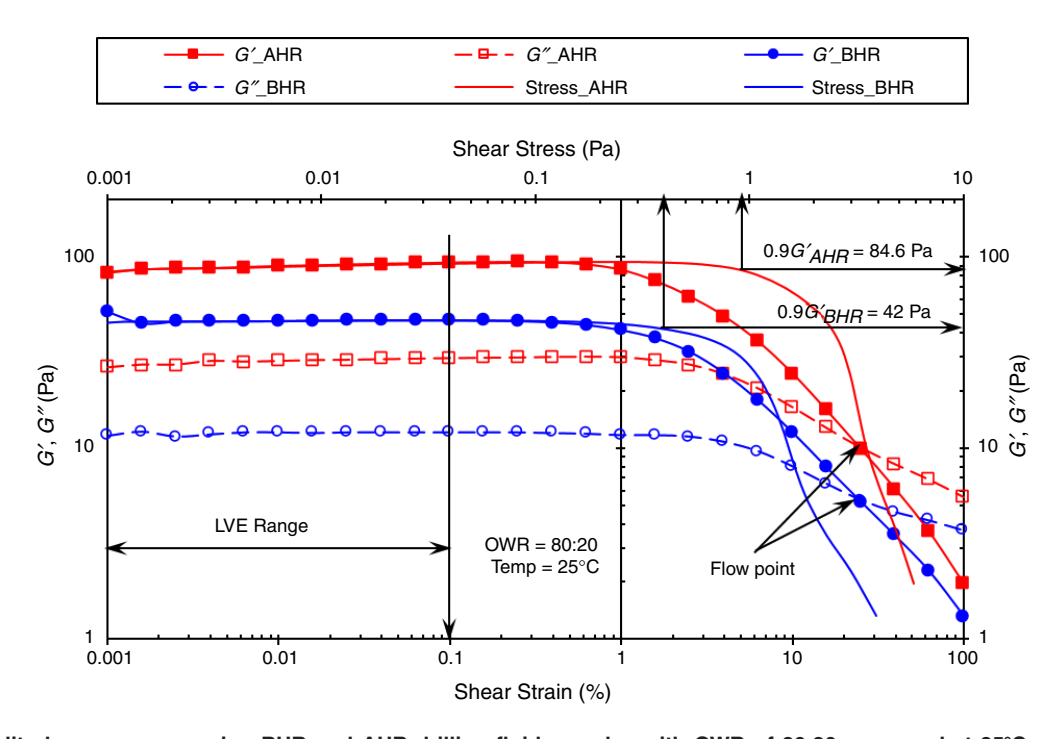


Fig. 9—Amplitude sweep comparing BHR and AHR drilling fluid samples with OWR of 80:20 measured at 25°C presented with shear strain and shear stress showing the limit of LVE range and flow point at G' = G'' at frequency of 10 rad/s.

Frequency Sweep. The frequency sweep provides information on the behavior and inner structure of the fluid sample as well as the long-term stability of dispersions. The required condition is that the selected shear strain amplitude is within the limit of LVE. For this study, a shear strain value of 0.05% was selected for analyzing the frequency sweep. As shown in Fig. 10, in a very long time (very low angular frequency, $\omega < 0.0015$ rad/s), the fluid sample after being hot-rolled exhibited a liquid behavior (G' > G') but maintained a solid behavior (G' > G'') as angular frequency increased. On the other hand, for the BHR fluid sample, a solid behavior is maintained over the entire range of angular frequency. The increasing trend of the storage modulus as angular frequency increased shows a weak gel structure of the fluid samples. In addition, the complex viscosity, in which the contribution of gel structure is included in the measured viscosity, decreased with increasing angular frequency. The G' and G'' measurements for the AHR fluid sample are always higher than the initial BHR fluid sample. With increased complex viscosity for the AHR fluid sample compared with the BHR fluid sample, possible long-term dispersion stability could occur, which could reduce barite sag potential. Fig. 11 illustrates that both fluid samples show viscoelastic behaviors because their phase shift angles δ are within 0 and 90°. This is also seen by the damping factor curves, which also indicate that the fluid samples are mostly entirely elastic because the damping factor, $\tan(\delta)$, is less than unity over the range of angular frequencies tested.

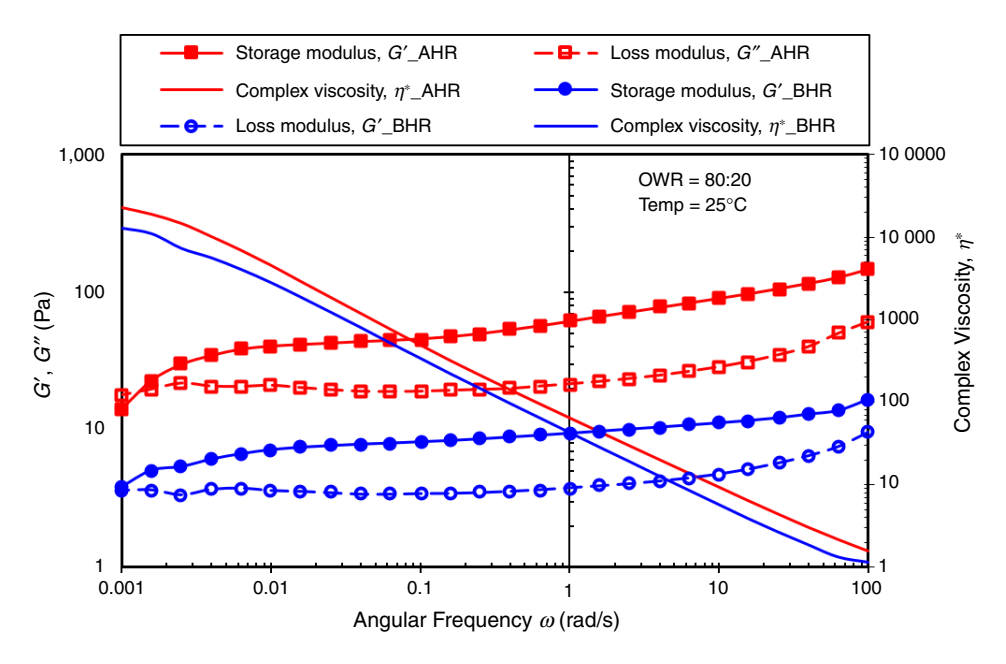


Fig. 10—Frequency sweep test comparing BHR and AHR drilling fluid samples with OWR of 80:20 measured at 25°C showing the loss and storage moduli as well as complex viscosity at LVE strain value of 0.05%.

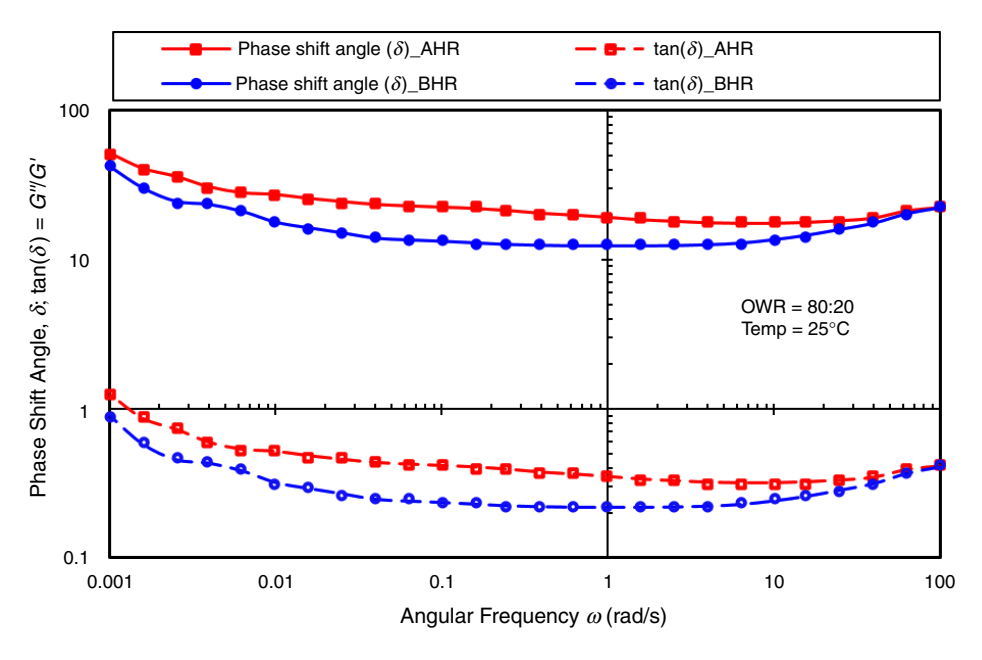


Fig. 11—Graph of phase shift angle and damping factor vs. angular frequency comparing BHR and AHR drilling fluid samples with OWR of 80:20 measured at 25°C at LVE strain value of 0.05%.

Analysis on Sag in OBDFs

Static Sag. Figs. 12 and 13, respectively, present the destabilization plots of the drilling fluid samples BHR and AHR in the form of the Δ BS curve against the height of the sample. As shown in Fig. 12, the Δ BS signal decreases at the top of the sample [marked as (c) to the right part of graph] due to a decrease of the concentration of barite particles, hence resulting in a more transparent section for the emitted light. At the bottom of the sample [marked as (a) to the left part of graph], there is a slight increase in Δ BS signal due to an increase in the barite particle concentration because of sediment formation. There is, however, little or no signal variation in the middle portion of the sample [marked as (b)], which indicates insignificant or no particle size variation. On the contrary, as presented in Fig. 13 for the AHR fluid sample, variations in the Δ BS signal occur at a sample height between 12 and 24 mm, which is a characteristic of the particle size variation, hence could be due to flocculation of barite particles and/or coalescence of water droplets. Again, similar signals are also shown at the top and bottom of the sample as was observed in Fig. 12. The most prominent feature of the data for both BHR and AHR samples is the strong drop in the Δ BS signal at the top, indicating a pure liquid layer. This layer could be due to syneresis. Particles and droplets may have agglomerated slightly, leaving a flow path to the top of the fluid column where the base oil has been allowed to migrate.

The migration rate or sedimentation velocity of the API barite particles in the drilling fluid was computed from a stability analyzer software using Eq. 2. The sedimentation process was observed as the thickness of the sediment layer increased with time at the bottom of the sample. **Fig. 14** shows the peak thickness vs. time. The peak thickness refers to the total height of the sediment layer with the change of time at the bottom of the sample. The migration rate can be expressed as the slope of the linear portion of the peak thickness curve. It is observed that the migration rate of the barite particles in the fluid system BHR was computed as 0.84 and 0.24 mm/d after

the fluid sample was hot-rolled (AHR). The inset figure shows the delay times of approximately 2 and 4 hours before the particles began to settle in the BHR and AHR fluid samples, respectively. After 7 days of analysis, the particle sediment thickness was recorded as 3.22 and 2.21 mm for the drilling fluid samples, BHR and AHR, as shown in Fig. 14. The observed characteristics show that the AHR fluid sample is more stable with less particle sediment thickness compared to the BHR fluid sample. This can further be attributed to the high storage modulus of AHR fluid sample, which indicates a stable gel structure to suspend the barite particles within the LVE range compared to the BHR fluid sample.

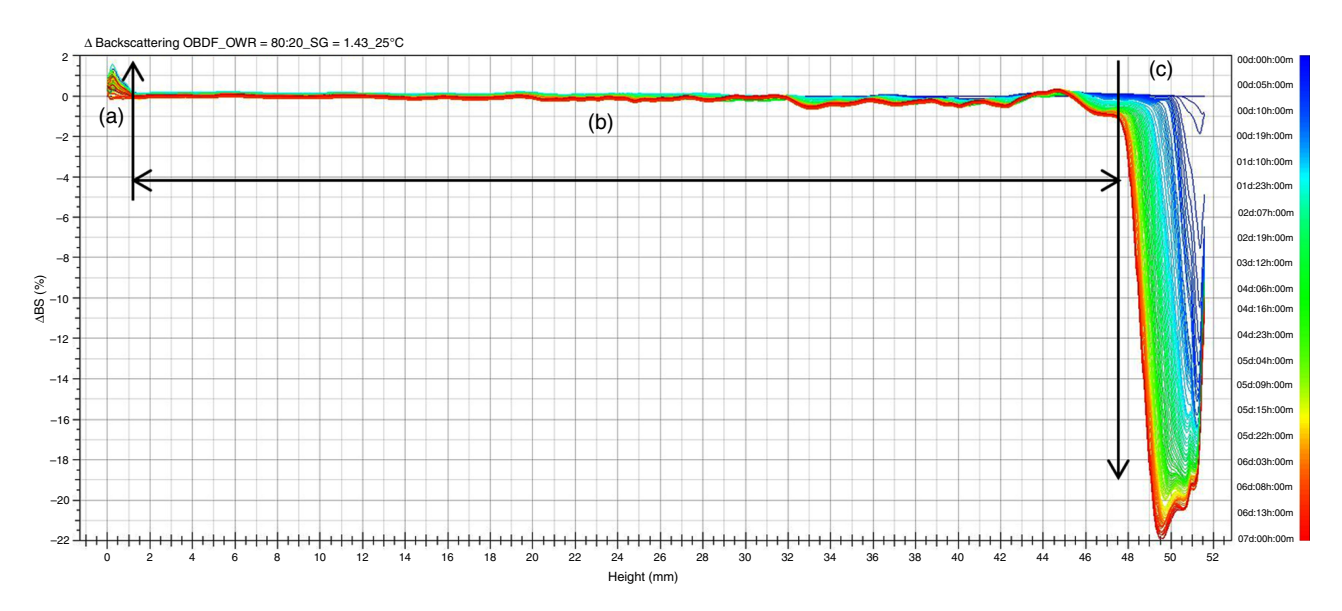


Fig. 12— Δ BS signal of BHR drilling fluid sample scanned for 7 days at 25°C. The height 0 mm indicates the bottom of the sample: (a) sedimentation, (b) no particle variation, and (c) clarification.

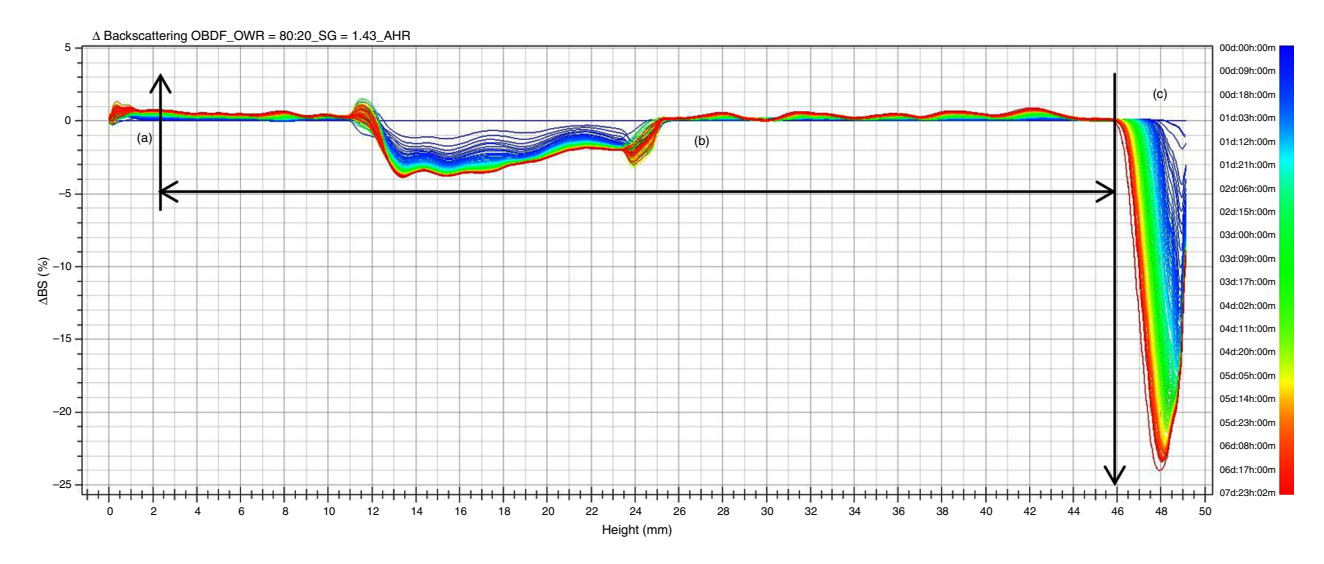


Fig. 13— Δ BS signal of AHR drilling fluid sample scanned for 7 days at 25°C. The height 0 mm indicates the bottom of the sample: (a) sedimentation, (b) particle size variation, and (c) clarification.

A further analysis on the stability of the dispersed barite particles in the drilling fluid sample was performed using the TSI. With the fluid sample that underwent a hot-rolled condition at 120°C for 60 hours, the TSI value was 1.0 as opposed to a TSI value of 3.0 for the BHR fluid sample as shown in Fig. 15. Using the TSI scale definition, the measured TSI value for the AHR fluid sample matched a TSI Scale B, indicating weak destabilization, whereas the measured TSI value for the BHR fluid sample matched a TSI Scale C, describing significant destabilization. It must be noted that the higher the TSI value, the less stable the fluid sample is, hence the faster the particles would settle. This further confirms that the AHR fluid samples are more stable than the BHR fluid samples.

To provide more insight into the static settling process in OBDFs, a gamma densitometer as shown in Fig. 4 was used with another fluid sample. This fluid sample was mixed according to the same composition and protocol as the fluid samples previously described. After hot rolling and thorough mixing, the fluid sample was transferred into a 2.5-cm diameter, 12-cm tall cylindrical column. Gamma scans were performed at four axial locations (1, 4, 6, and 8 cm from the bottom of the test cell) by moving the source and detector vertically. Fig. 16 shows the changes in the barite volume fraction obtained from the gamma beam scans at four axial locations. The attenuation decreases when the local particle density in the drilling fluid decreases. It is evident from the figure that the solid fraction decreased at an axial location of 8 cm (near the top of the test cell) with time due to the gravitational settling of high-density barite particles. Fig. 16a shows the change in the solid fraction for the first 1,000 minutes after the start of the experiment. It is clear that the particles began to settle almost immediately near the top of the cell (at 8 cm from the bottom of the cell), and most of the drop in the fluid

density had occurred after 500 minutes (approximately 8 hours). On the other hand (Fig. 16b), the solid fraction and the fluid density at lower axial locations (1, 4, and 6 cm from the bottom) changed (increased) more slowly and reached steady state with time. Interestingly, the increment in the fluid density was approximately the same at all three axial locations, and it can be attributed to the gelforming nature of the hot-rolled drilling fluid.

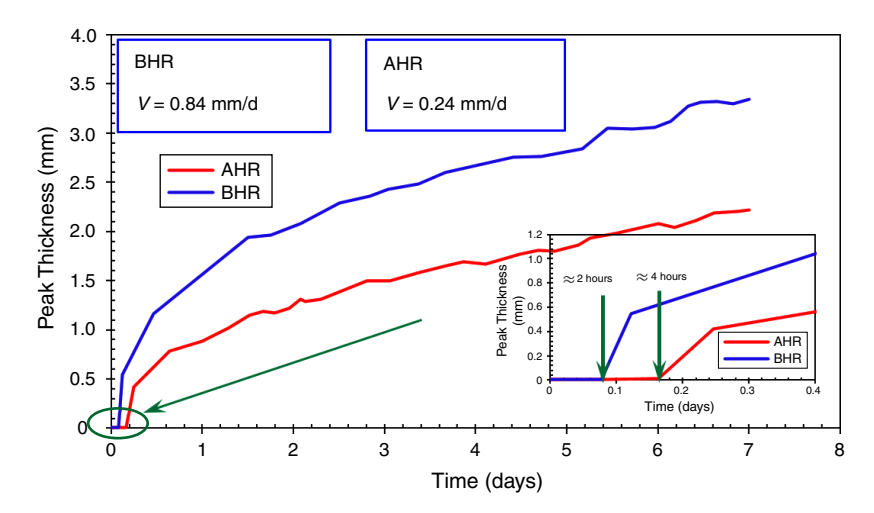


Fig. 14—Peak thickness of API barite particles of BHR and AHR drilling fluid samples measured over a period of 7 days at 25°C. The inset figure shows the delay time for particles to settle.

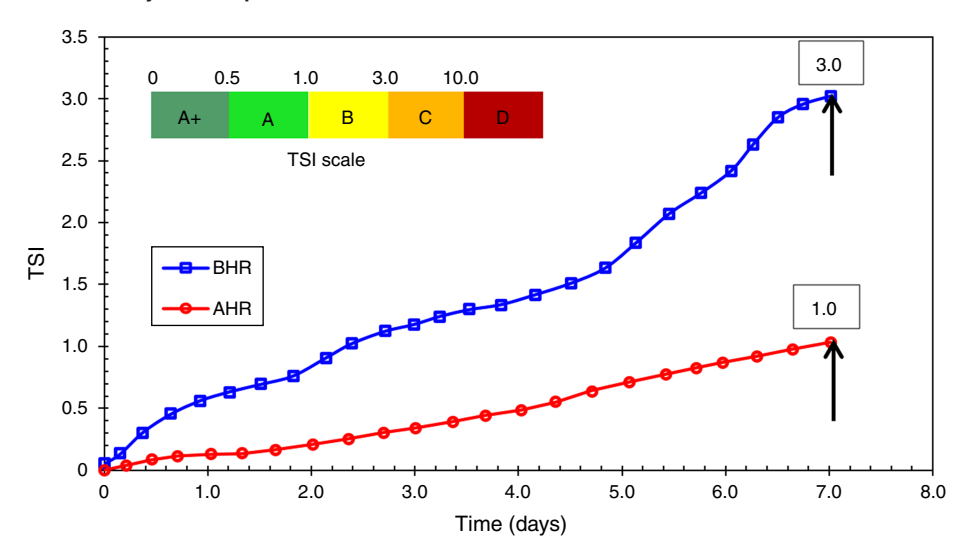


Fig. 15—TSI of dispersed barite particles in drilling fluid sample for BHR and AHR conditions measured over a period of 7 days at 25°C.

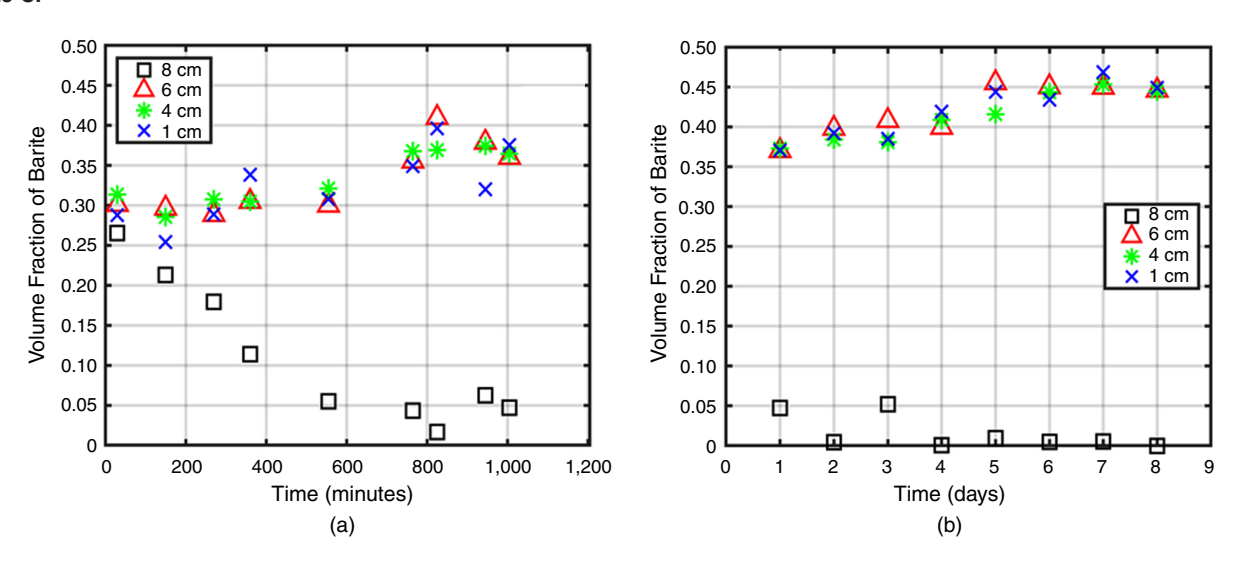


Fig. 16—Change in barite volume fraction with time at different heights from the bottom of the test cell: (a) over the first 1,000 minutes on the first day and (b) over the duration of 8 days.

Dynamic Sag. Rotational shear viscosity vs. time plots for various shear rates are presented in **Fig. 17** for the BHR and AHR fluid samples for a time period of 10,800 seconds; however, only the early time results are presented. It is observed that the lowest shear rate value of 0.001 s⁻¹ resulted in the highest viscosity values, whereas the highest shear rate value of 10.22 s⁻¹ gave the lowest viscosity values with time for both BHR and AHR fluid samples. Furthermore, the viscosity values of the AHR fluid sample at each shear rate was higher than those of the BHR fluid sample. It is worth noting that as the shear rate increases, the time required for a steady-state viscosity to be reached decreases. This implies that a considerable thixotropic effect is displayed at low shear rates in which more time is required to achieve steady-state condition. On the contrary, there is only a small thixotropic effect at high shear rates as indicated by very short times required to achieve steady state (Varges et al. 2019).

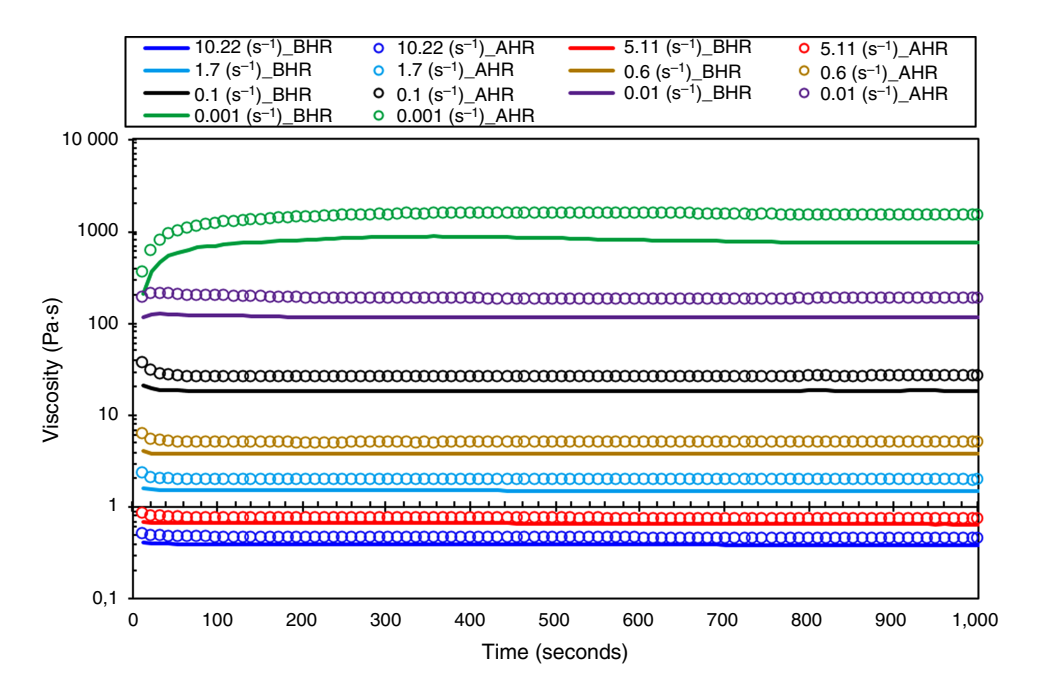


Fig. 17—Steady shear viscosity/time sweep test for both BHR and AHR fluid samples at 25°C.

As previously mentioned, the DSI is defined as the initial drilling fluid density divided by twice the final density taken from the top of the sample. The effects of rotational shear and oscillatory shear on the sag potential of the drilling fluid sample at constant strain amplitudes of 0.05 (within LVE range) and 100% were analyzed. Fig. 18 presents the BHR fluid sample results that show there is low barite sag tendency from a shear rate of 0.001 to 0.60 s⁻¹, which is within the favorable region to avoid sag with the DSI range of 0.50 to 0.51 for the conditions of rotational shear and oscillatory shear at 100% strain amplitude. At higher strain or shear rates than approximately 1.0 s⁻¹, there is a dramatic increase in barite sag potential with maximum DSI values of 0.566 and 0.537 recorded for the conditions of rotational shear at 10.22 s⁻¹ and oscillatory shear at 10.22 rad s⁻¹ of 100% strain amplitude, respectively. It is, however, observed that the impact of oscillatory shear at a constant strain amplitude of 0.05% (within LVE range) resulted in low barite sag potential within the favorable region to avoid sag of DSI over the entire range of angular frequencies. It should be noted that within the LVE range, we do not disturb the particle positions enough to promote sag. With reference to no sag condition (that is, DSI ≈ 0.50), there is an increase in sag tendencies by 1.4% for oscillatory shear within the LVE range, 7.4% for oscillatory shear at maximum amplitude strain, and 13.2% for rotational shear, all at 10.22 s⁻¹. It is indicated that sag tendencies are more pronounced during rotational shear as compared to oscillatory shear. In this study, a DSI greater than 0.51 is considered as the region vulnerable to sag, whereas a DSI less than 0.51 indicates a favorable sag region. For a perfect stable drilling fluid sample with no sag, DSI equals 0.50. It should be noted that DSI values less than 0.50 might result from limitations in measurement accuracy. These values imply negative sag, which could occur for nanoparticles or by flotation if certain gases are dissolved.

In Fig. 19, we compare the effects of rotational shear and oscillatory shear at 100% on the DSI for the AHR drilling fluid sample. The results show an insignificant barite sag occurring below $1.0~\rm s^{-1}$ for rotational shear and $3.0~\rm rad/s$ for oscillatory shear due to the high stability of the drilling fluid sample. Above these shear rates, however, dynamic sag exceeded the favorable region to avoid sag with rotational shear exhibiting more sag than the oscillatory shear. There is an increase in sag tendency by $6.0~\rm and~9.8\%$ for oscillatory shear at maximum amplitude strain and rotational shear, respectively, at $10.22~\rm s^{-1}$ (or $10.22~\rm rad/s$), with reference to no sag condition (DSI ≈ 0.50). Sag tendency is more evident by rotational shear as compared to oscillatory shear, especially at shear rates between $1.0~\rm and~10.22~\rm s^{-1}$.

A comparative analysis between drilling fluid samples BHR and AHR at rotational shear condition is presented in **Fig. 20.** A similar comparison using oscillatory shear at amplitude strain of 100% is shown in **Fig. 21.** For the rotational shear comparison, the AHR fluid sample recorded a low barite sag potential over the entire range of shear rates compared to the BHR fluid sample. For both fluid samples, the performance of barite sag is nonetheless within the favorable region to avoid sag below a rotational shear rate of $1.0 \, \text{s}^{-1}$ as presented in Fig. 20. On the other hand, during oscillatory shear, the barite sag performance of the BHR and AHR fluid samples was similar only within the angular frequency range of 0.001 to 0.10 rad/s. Afterward, the sag tendency in the BHR fluid sample exceeded that of the AHR fluid sample as shown in Fig. 21. Increases in the barite sag index by 7.4 and 6.0% are recorded for BHR and AHR fluid samples, respectively, with reference to no sag condition (DSI \approx 0.50). The reason is that hot rolling the sample activates the viscosifiers contributing to an increase in viscosity.

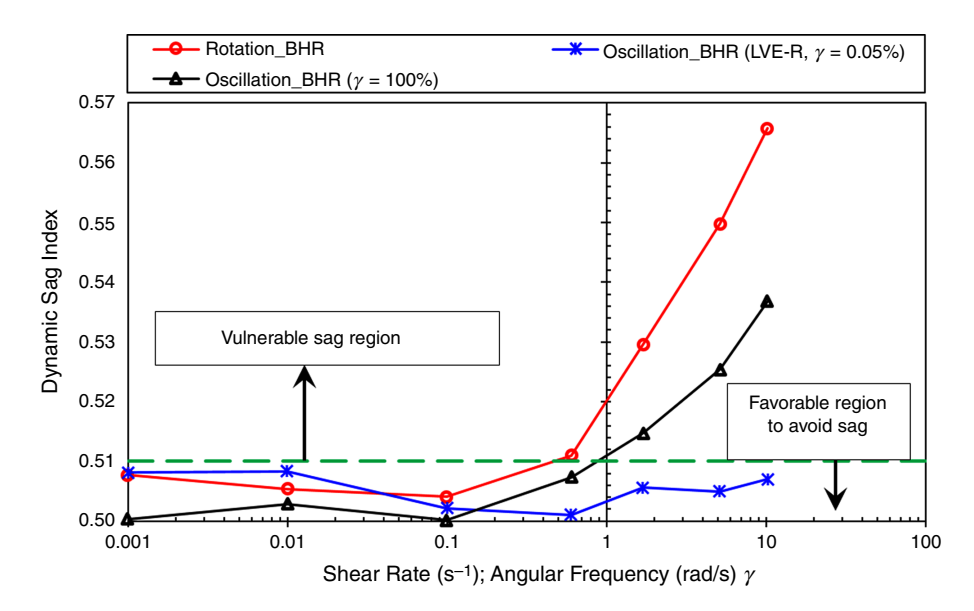


Fig. 18—DSI of the BHR drilling fluid sample measured at different dynamic conditions at 25°C: rotational shear, oscillatory shear at 0.05%, and 100% amplitude shear strain.

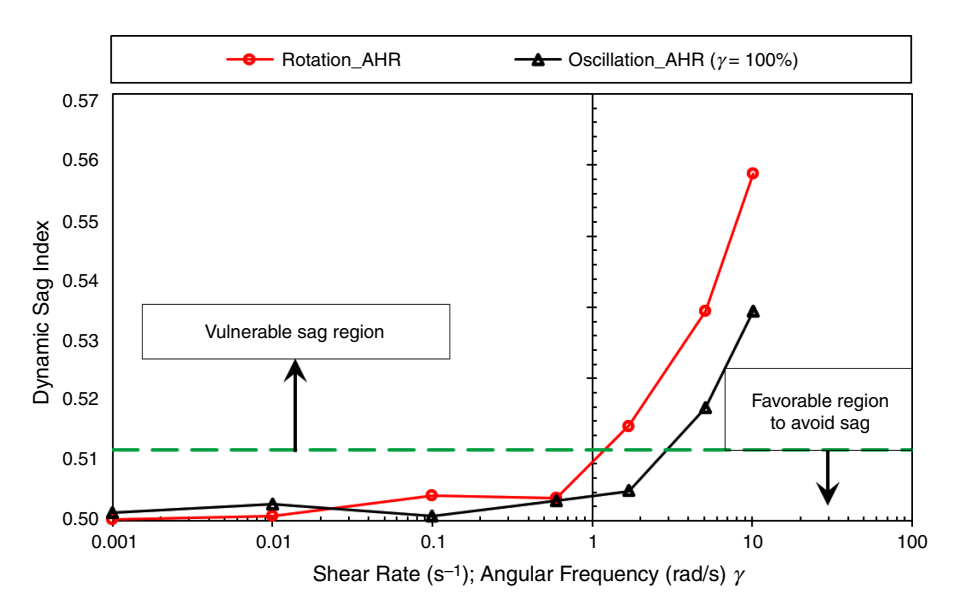


Fig. 19—DSI of AHR drilling fluid sample measured at rotational shear and oscillatory shear with 100% amplitude shear strain at 25°C.

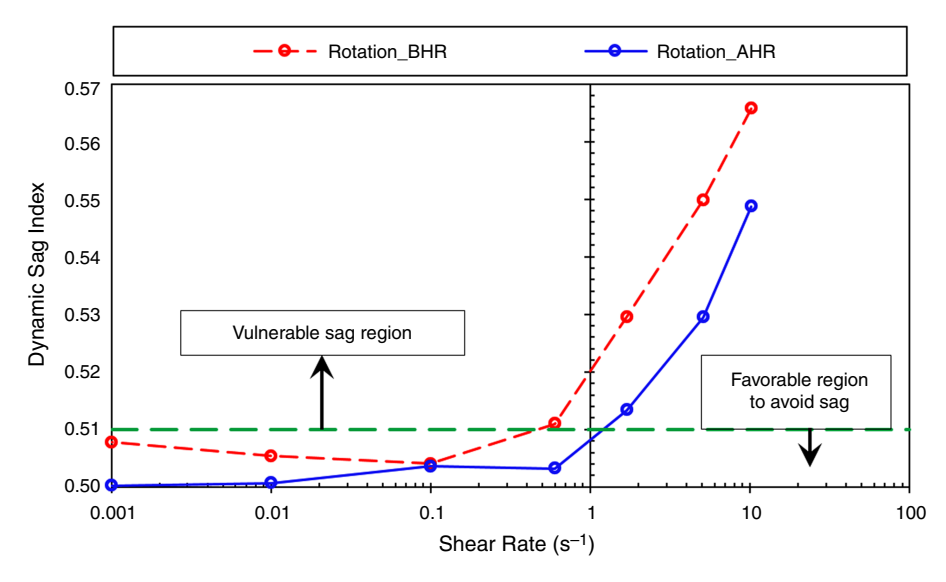


Fig. 20—DSI comparison between BHR and AHR drilling fluid sample measured under rotational shear at 25°C.

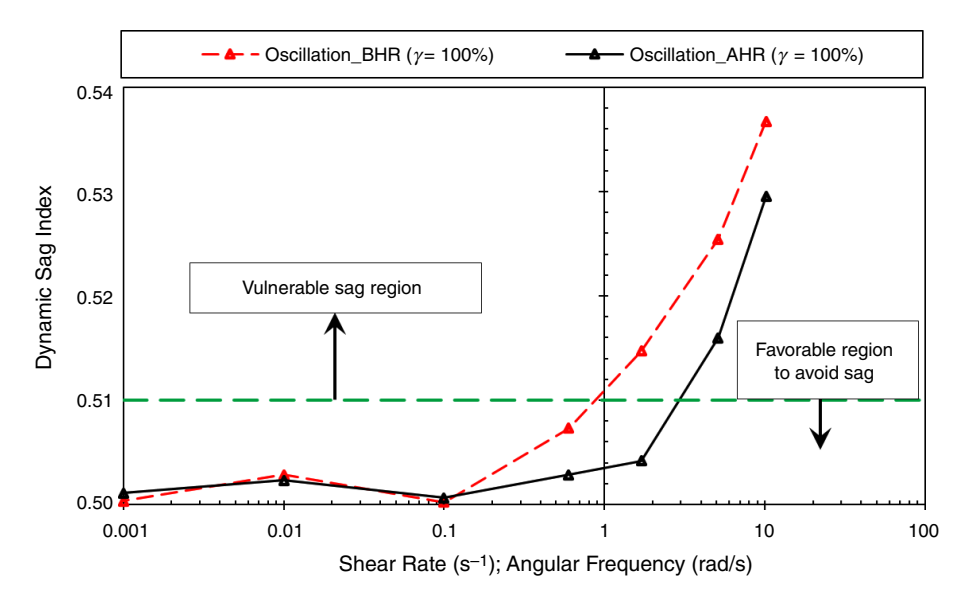


Fig. 21—DSI comparison between BHR and AHR drilling fluid sample measured under oscillatory shear at 25°C.

Sag Density. Presented in Figs. 22 and 23 are the comparisons of dynamic sag densities, $\Delta \rho$ (g/cm³) calculated using Eq. 6 between the BHR and AHR fluid samples measured after a 3-hour constant shear at both rotational and oscillatory shear conditions. When increasing the shear rate from 0.001 to $10.22 \, \mathrm{s}^{-1}$, the sag density ($\Delta \rho$) increased with hot rolling, except from 0.1 to $0.6 \, \mathrm{s}^{-1}$ as shown in Fig. 22. A similar result was also observed by Nguyen et al. (2011). For the fluid sample BHR, there is a dramatic increase in sag density from shear rate of 0.1 to $10.22 \, \mathrm{s}^{-1}$; however, decreasing the shear rate below $0.1 \, \mathrm{s}^{-1}$ seemed to slightly promote sag because we recorded a slight increase in the sag density, as presented in Fig. 22. This is an indication that increasing the shear rate promotes sag in the fluid samples. A sag density close to zero indicates that the barite particles are in full suspension in the fluid sample. Overall, less sag was recorded in the fluid sample AHR than BHR for all shear rates. To simulate the impact of vibration by the drillstring on sag density, we present in Fig. 23 the results for oscillatory shear at strain amplitude of 100%. For fluid samples BHR and AHR, a dramatic sag density was recorded from 0.1 to $10.22 \, \mathrm{rad/s}$ with severe sag occurring in the fluid sample BHR. However, below 0.1 rad/s the performance of both fluid samples with regard to sag was quite similar.

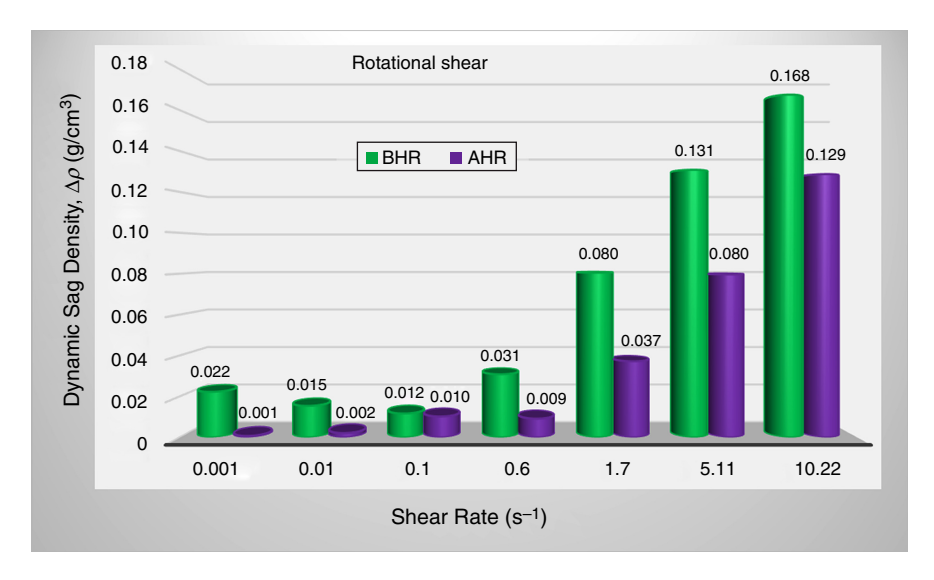


Fig. 22—Dynamic sag density between BHR and AHR drilling fluid samples measured after 3 hours under constant rotational shear at 25°C.

To measure the sag density (also referred to here as a change in the fluid density) as a function of time, we adopted a technique by Tehrani et al. (2011), which is expressed in terms of the change in the bulk density of the fluid in the rheometer gap. The expression is as follows:

$$\delta\rho(t) = \rho(0) \left[\frac{\tau(0) - \tau(t)}{\tau(0)} \right], \qquad (19)$$

where $\delta \rho$ is the change in fluid density (g/cm³), $\rho(0)$ is the initial density of the fluid sample, $\tau(0)$ is the initial shear stress in Pa, and $\tau(t)$ is the shear stress as a function of time.

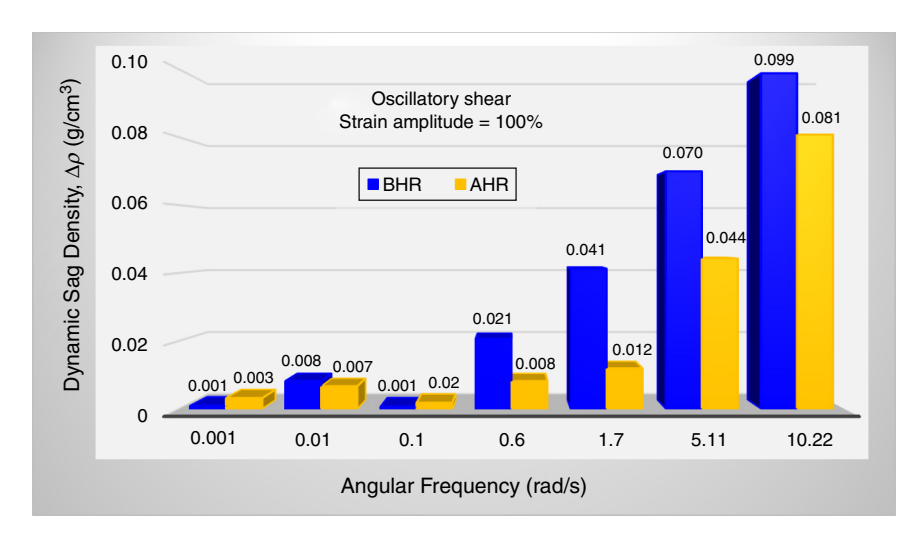


Fig. 23—Dynamic sag density between BHR and AHR drilling fluid samples measured after 3 hours under constant oscillatory shear and strain amplitude of 100% at 25°C.

In **Fig. 24**, the results are presented for fluid samples BHR and AHR with continuous rotational shear at 10.22 s⁻¹. Fig. 24 shows that at previous times, the rate of drop in fluid density increases faster but decreases gradually with time. The change in the fluid density with time is, however, more dramatic at previous times for the hot-rolled fluid sample as shown in the inset figure. We believe that under a rotational shear condition, barite particles will settle. The settling will first occur at a faster rate with the large size particles. This behavior occurs at previous times as can be seen in Fig. 24. This would result in high-density difference within the fluid column. The drop rate in fluid density decreases with increasing time because small-size particles settle at a slower rate. A comparison between Figs. 22 and 24 at a shear rate of $10.22 \, \mathrm{s^{-1}}$ indicates a dramatic difference in the change in fluid density measured according to Eqs. 6 and 19. For instance, after 3 hours of continuous rotational shear, Eq. 6 recorded a change in the fluid density of 0.168 and 0.129 g/cm³ as opposed to 0.330 and 0.291 g/cm³ with Eq. 19 for BHR and AHR fluid samples, respectively. If we measure the change in the fluid density at approximately 1,000 seconds from Fig. 24, we obtain a similar value for BHR fluid from Fig. 22; however, a high value is obtained for the AHR fluid sample at the same measuring time. It should be noted that this technique could generate conservative results due to the assumption that the rate of particle settling is uniform with time in the rheometer gap. However, the rheological and viscoelastic complexities of these fluid samples in addition to their variable PSDs are some factors that can enhance nonuniform particle settling behavior in the rheometer gap. Nonetheless, this technique is adequate for monitoring sag performance as a function of time and offers a high degree of reproducibility and reliability of sag density.

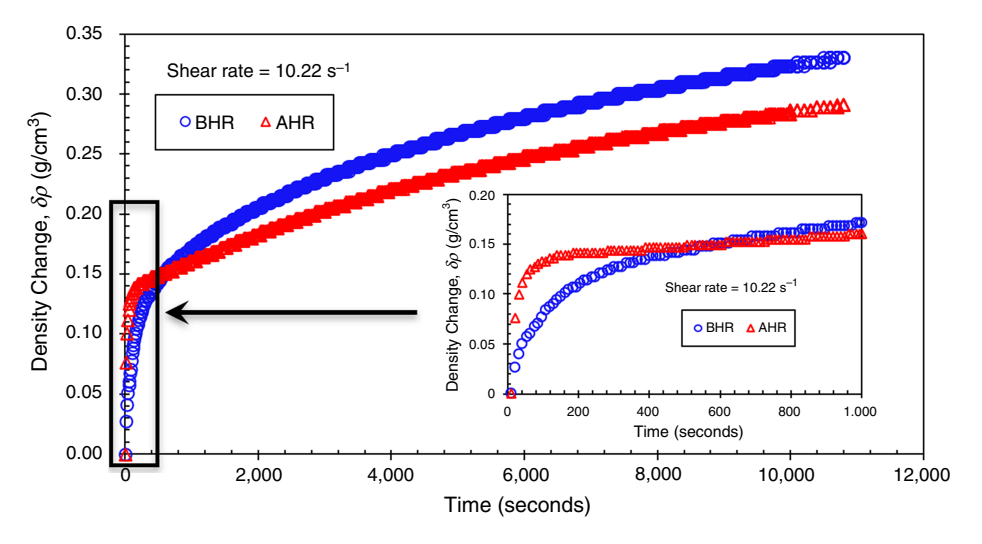


Fig. 24—Change in fluid density for BHR and AHR fluid samples at a shear rate of 10.22 s⁻¹.

Time-Dependent Sweep Analysis. To further confirm the existence of barite sag in the drilling fluid samples, time-dependent oscillatory shear tests (i.e., with constant frequency and amplitude) were conducted to analyze barite sag potential in the BHR and AHR drilling fluid samples using the storage modulus G' data. These tests aim to simulate the effect of drillstring vibration on the sag potential of the drilling fluid samples. The storage modulus G' reflects the elastic behavior of the fluid. As shown in **Fig. 25**, the characteristic profile of the storage modulus for the BHR fluid sample within the LVE range at an amplitude strain of 0.05% and a frequency of 10.22 rad/s showed an initial structural buildup up to a time period of 3,600 seconds and a sharp decline afterward. This indicates gel growth in the fluid sample up to 3,600 seconds and a breakdown of the fluid's gel structure after 3,600 seconds. Therefore, the fluid sample at rest should be recirculated within 3,600 seconds, or else particles would aggregate and settle down. On the contrary, the characteristic profile of the AHR fluid sample showed a continuous increase in storage modulus over the entire time period, an indication of strong gel structure of the fluid sample, as also illustrated in Fig. 25.

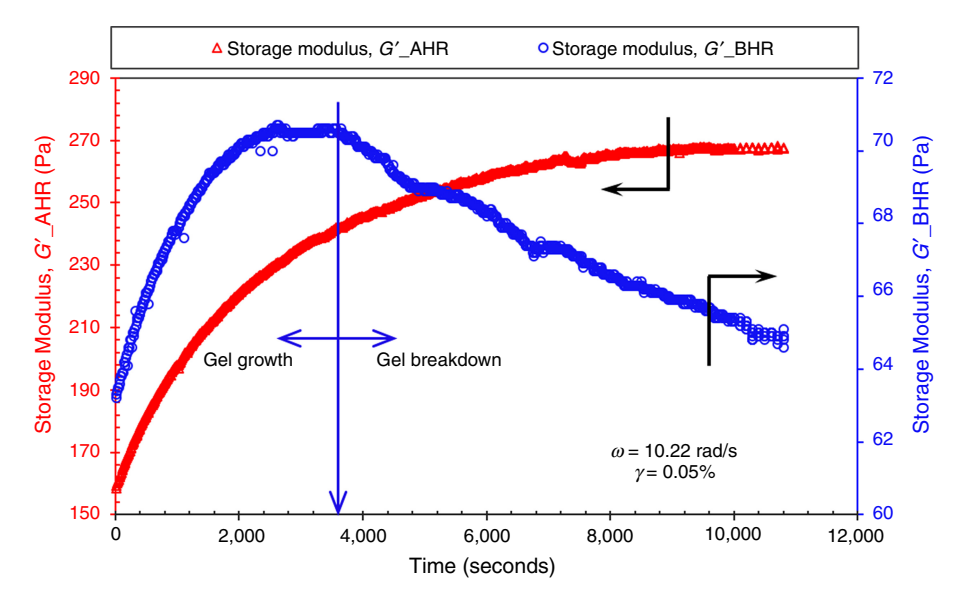


Fig. 25—Time-dependent oscillatory shear analysis of BHR and AHR drilling fluid samples showing the characteristic profiles of the storage modulus within the LVE range at an amplitude strain of 0.05% and angular frequency of 10.22 rad/s measured at 25°C.

A maximum strain amplitude of 100% was imposed on the fluid systems with an angular frequency of 10.22 rad/s for both BHR and AHR fluid samples, and the characteristic curves of the storage modulus G' for the BHR and AHR fluid samples are presented in Fig. 26. It is observed that the AHR fluid sample initially registered an initial measurement noise with a sharp decrease in G' up to approximately 400 seconds, and hence can be disregarded. This behavior was also present from the shear stress amplitude values at the start of the measurements and then adjusted with time. The G' curve of the BHR fluid sample shows a continuous decline, although gradually, thus indicating a continual gel breakdown in the fluid structure and a potential for promoting sag. However, the G' curve of the AHR fluid sample, after the initial measurement noise, shows a gradual gel structural buildup with time. This phenomenon explains why the AHR fluid sample limited the occurrence of barite sag as compared to the BHR fluid sample.

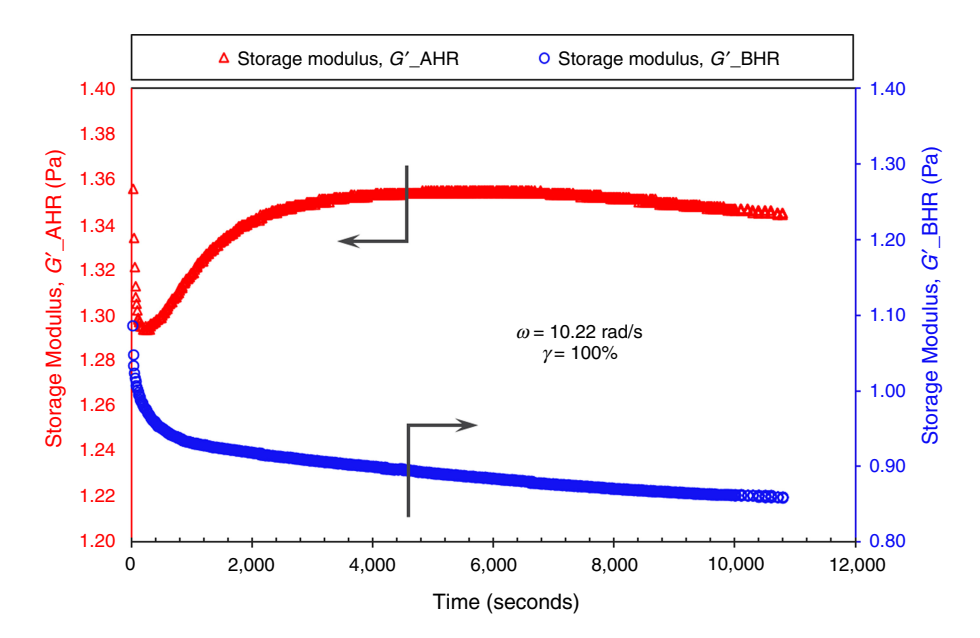


Fig. 26—Time-dependent oscillatory shear analyses of BHR and AHR drilling fluid samples showing the characteristic profiles of the storage moduli at amplitude strain of 100% and angular frequency of 10.22 rad/s measured at 25°C.

Conclusions

We have presented a comprehensive barite sag study on OBDF samples, BHR and AHR. Barite sag of a liquid column under static conditions has been characterized using LS measurements, hydrostatic pressure measurements, and gamma densitometry. Barite sag in a sheared liquid column has been characterized by using a rotating cylinder rheometer to produce oscillatory and rotational shear. All tests were accompanied by extensive rheological characterization of the fluids using the rotating cylinder rheometer. The experiments reported here have been conducted in two different laboratories, with different measurement equipment and methods, but using the same drilling fluid. The drilling fluid was prepared in the respective laboratories using the same recipes and mixing protocols, with the same components from the same supplier.

From the results obtained in this study, the following conclusions can be drawn:

- 1. A comparison of hydrostatic pressure and gamma densitometer measurements in a barite particle-water mixture under static conditions showed overall consistent results concerning the barite particle sedimentation behavior over time. The comparison however also showed the limitation of the pressure method, which should therefore be used with caution. Taking this into account, these methods should also be suitable for characterization of barite sag in drilling fluids.
- 2. Both viscosity and viscoelastic-linear elasticity changed to higher values AHR the OBDF sample.
- 3. In the static sag test using the optical stability analyzer, high viscoelastic elasticity of the hot-rolled fluid sample contributed to lower particle settling rates and longer dispersion times than the sample BHR.
- 4. In the dynamic sag test, rotational shear promoted barite sag more readily than oscillatory shear for both sample treatments; BHR and AHR fluid samples.
- 5. Chemicals heat activated by the hot-rolling process increased the viscosity and elasticity and reduced the barite sag for the fluid sample.
- 6. Within the LVE range, the barite sag remained in a favorable region to avoid sag with a DSI = 0.50 to 0.51 over the entire shear rate during oscillatory shear. The oscillatory shear test did not disturb the position of the particles enough to promote sag in the fluid samples.
- 7. Sag is more severe in fresh-made fluid samples than in fluid samples AHR in which a dramatic sag density ($\Delta \rho$) occurred from increasing the rotational shear rate from 0.1 to 10.22 s⁻¹.
- 8. Time-dependent oscillatory shear analysis of the elasticity of the fluid sample can provide valuable information on the breakdown and growth of microstructures in the drilling fluid samples to predict the occurrence of barite sag.
- 9. Barite sag is a complex process even under static conditions. Both Turbiscan and gamma densitometry measurements show the development of a solids-free layer at the top. The formation of this region is likely due to syneresis. Syneresis has not been evaluated in this study. Gamma densitometry indicates a more or less uniform compaction of the barite in the fluid below the liquid layer. Turbiscan measurements show a delay in the initiation of settling in static fluid not seen from the gamma densitometry measurements. This delay is longer when the fluid is hot-rolled.

Acknowledgments

This work was carried out at the laboratories of NTNU and SINTEF in Norway and the laboratories at CUNY in New York. We acknowledge the financial support of the Research Council of Norway and the National Science Foundation of USA under Award Number 1743794 for the PIRE project "Multiscale, Multiphase Phenomena in Complex Fluids for the Energy Industries." Special thanks to M-I SWACO, Schlumberger Norge AS for supplying the drilling fluid chemicals and providing technical support.

References

Al-Bagoury, M. and Steele, C. 2012. A New, Alternative Weighting Material for Drilling Fluids. Paper presented at the IADC/SPE Drilling Conference and Exhibition, San Diego, California, USA, 6–8 March SPE-151331-MS. https://doi.org/10.2118/151331-MS.

Baldino, S., Osgouei, R. E., Ozbayoglu, E. et al. 2018. Quemada Model Approach to Oil or Synthetic Oil Based Drilling Fluids Rheological Modelling. J Pet Sci Eng 163: 27–36. https://doi.org/10.1016/j.petrol.2017.12.042.

Bamberger, J. A., Greenwood, M. S., and Kytomaa, H. K. 1998. *Ultrasonic Characterisation of Slurry Density and Particle Size*. New York, New York, USA: American Society of Mechanical Engineers.

Beckman Coulter, Inc. 2011. LS Series Product Manual. Pasadena, California, USA: Beckman Coulter, Inc.

Boycott, A. E. 1920. Sedimentation of Blood Corpuscles. Nature 104: 532. https://doi.org/10.1038/104532b0.

Cayeux, E. 2020. Time, Pressure and Temperature Dependent Rheological Properties of Drilling Fluids and Their Automatic Measurements. Paper presented at the IADC/SPE International Drilling Conference and Exhibition, Galveston, Texas, USA, 3–5 March. SPE-199641-MS. https://doi.org/10.2118/199641-MS.

Dickinson, E. 1992. An Introduction to Food Colloids, 82–86. Oxford, England, UK: Oxford Science Publishing,

Dixmier, M. 1978. A New Description of Random Stacks and Dense Fluids. *J Phys France* **39** (8): 873–895. https://doi.org/10.1051/jphys:01978003908087300.

Dye, W., Hemphill, T., Gusler, W. et al. 2001. Correlation of Ultralow-Shear-Rate Viscosity and Dynamic Barite Sag. SPE Drill & Compl 16 (1): 27–34. SPE-70128-PA. https://doi.org/10.2118/70128-PA.

Ehrhorn, C. and Saasen, A. 1996. Barite Sag in Drilling Fluids. *Ann Trans Nordic Rheol Soc* 4: 66–68. https://nordicrheologysociety.org/Content/Transactions/1996/vol.4_ehrhorn.pdf.

Formulaction. 2008. Turbiscan Lab User Guide, Edition 5. Worthington, Ohio, USA: Formulaction.

Hold, S. 2015. The Very Basics of Density Measurement Methods. Anton Paar Blog, https://blog.anton-paar.com/the-very-basics-of-density-measure-ment/.20/10/19.

Jachnik, R. 2005. Drilling Fluid Thixotropy & Relevance. Ann Trans Nordic Rheol Soc 13: 121–126. https://nrs.blob.core.windows.net/pdfs/nrspdf-7d16161f-f740-49ce-9ece-3a96d70cf6e1.pdf.

Jamison, D. E. and Clements, W. R. 1990. A New Test Method to Characterize Setting/Sag Tendencies of Drilling Fluids Used in Extended Reach Drilling. ASME Drill Technol Symp (27): 109–113.

Jefferson, D. T. 1991. New Procedure Helps Monitor Sag in the Field. Paper presented at the Energy Sources Technology Conference and Exhibition, New Orleans, Louisiana, USA, 20–24 January.

Liu, Z. Q., Yang, X., and Zhang, Q. 2014. TURBISCAN: History, Development, Application to Colloids and Dispersion. *Adv Mater Res* **936**: 1592–1596. https://doi.org/10.4028/www.scientific.net/AMR.936.1592.

Lu, Y., Kang, W., Jiang, J. et al. 2017. Study on the Stabilization Mechanism of Crude Oil Emulsion with an Amphiphilic Polymer Using the β-Cyclodextrin Inclusion Method. RSC Adv 7 (14): 8156–8166. https://doi.org/10.1039/C6RA28528G.

Marshall, D. S. 2007. Laboratory Investigation of Barite Sag in Drilling Fluids. *Ann Trans Nordic Rheol Soc* (15). https://nrs.blob.core.windows.net/pdfs/nrspdf-8c32fcf5-340c-49bd-be4b-3d11fc5ae5d4.pdf.

Maxey, J. 2007. Rheological Analysis of Static and Dynamic Sag in Drilling Fluids. *Ann Trans Nordic Rheol Soc* (15): 181–188. https://nrs.blob.core. windows.net/pdfs/nrspdf-f3741626-0a14-4902-8c2a-aaa94c73eb68.pdf.

Mezger, T. G. 2014. The Rheology Handbook, fourth edition. Hannover, Germany: Vincentz Network.

Mill, P. and Snabre, P. 1994. Settling of a Suspension of Hard Spheres. *Europhys Lett* 25 (9): 651–656. https://doi.org/10.1209/0295-5075/25/9/003.

- Moreira, B. A., de Oliveira Arouca, F., and Damasceno, J. J. R. 2017. Analysis of Suspension Sedimentation in Fluids with Rheological Shear-Thinning Properties and Thixotropic Effects. *Powder Technology* **308**: 290–297. https://doi.org/10.1016/j.powtec.2016.12.034.
- Nguyen, T., Miska, S., Yu, M. et al. 2011. Experimental Study of Dynamic Barite Sag in Oil-Based Drilling Fluids Using a Modified Rotational Viscometer and a Flow Loop. *J Pet Sci Eng* **78** (1): 160–165. https://doi.org/10.1016/j.petrol.2011.04.018.
- Nguyen, T. C., Miska, S., Saasen, A. et al. 2014. Using Taguchi and ANOVA Methods to Study the Combined Effects of Drilling Parameters on Dynamic Barite Sag. *J Pet Sci Eng* **121**: 126–133. https://doi.org/10.1016/j.petrol.2014.06.029.
- Ofei, T. N., Lund, B., Saasen, A. et al. 2019. A New Approach to Dynamic Barite Sag Analysis on Typical Field Oil-Based Drilling Fluid. *Ann Trans Nordic Rheol Soc* (27): 61–69. https://nrs.blob.core.windows.net/pdfs/nrspdf-bbf992e3-cf87-4ab0-8bc3-88184ba03e1b.pdf.
- Ofei, T. N., Lund, B., Saasen, A. et al. 2020. Barite Sag Measurements. Paper presented at the IADC/SPE International Drilling Conference and Exhibition, Galveston, Texas, USA, 3–5 March. SPE-199567-MS. https://doi.org/10.2118/199567-MS.
- Omland, T. H., Albertsen, T., Taugbøl, K. et al. 2006. The Effect of the Synthetic- and Oil-Based Drilling Fluid's Internal Water-Phase Composition on Barite Sag. SPE Drill & Compl 21 (2): 91–98. SPE-87135-PA. https://doi.org/10.2118/87135-PA.
- Omland, T. H., Saasen, A., and Amundsen, P. A. 2007. Detection Techniques Determining Weighting Material Sag in Drilling Fluid and Relationship to Rheology. *Ann Trans Nordic Rheol Soc* 15: 1–9. https://nrs.blob.core.windows.net/pdfs/nrspdf-a5b9f18e-7a1e-46dc-adca-75a4a27ef91b.pdf.
- Omland, T. H., Saasen, A., Zwaag, CV. et al. 2007. The Effect of Weighting Material Sag on Drilling Operation Efficiency. Paper presented at the Asia Pacific Oil and Gas Conference and Exhibition, Jakarta, Indonesia, 30 October–1 November. SPE-110537-MS. https://doi.org/10.2118/110537-MS.
- Parvizinia, A., Ahmed, R. M., and Osisanya, S. O. 2011. Experimental Study on the Phenomenon of Barite Sag. Paper presented at the International Petroleum Technology Conference, Bangkok, Thailand, 15–17 November. IPTC-14944-MS. https://doi.org/10.2523/IPTC-14944-MS.
- Quemada, D. 1998. Rheological Modelling of Complex Fluids. I. The Concept of Effective Volume Fraction Revisited. Eur Phys J Appl Phys 1 (1): 119–127. https://doi.org/10.1051/epjap:1998125.
- Rocha, R. R., Oechsler, B. F., Meleiro, L. A. et al. 2020. Settling of Weighting Agents in Non-Newtonian Fluids to Off-Shore Drilling Wells: Modeling, Parameter Estimation and Analysis of Constitutive Equations. *Journal of Petroleum Science and Engineering* 184: 106535. https://doi.org/10.1016/j.petrol.2019.106535.
- Saasen, A., Liu, D., and Marken, C. D. 1995. Prediction of Barite Sag Potential of Drilling Fluids from Rheological Measurements. Paper presented at the SPE/IADC Drilling Conference, Amsterdam, The Netherlands, 28 February–2 March. SPE-29410-MS. https://doi.org/10.2118/29410-MS.
- Saasen, A., Marken, C., Sterri, N. et al. 1991. Monitoring of Barite Sag Important in Deviated Drilling. Oil & Gas J 89 (34): 43-50.
- Santos, N. B. C., Fagundes, F. M., de Oliveira Arouca, F. et al. 2018. Sedimentation of Solids in Drilling Fluids Used in Oil Well Drilling Operations. *Journal of Petroleum Science and Engineering* **162:** 137–142. https://doi.org/10.1016/j.petrol.2017.12.026.
- Savari, S., Kulkarni, S., Maxey, J. et al. 2013. A Comprehensive Approach to Barite Sag Analysis on Field Muds. Paper presented at the AADE National Technical Conference and Exhibition, Oklahoma City, Oklahoma, USA, 26–27 February.
- Skalle, P., Backe, K. R., Lyomov, S. K. et al. 1999. Barite Segregation in Inclined Boreholes. J Can Pet Technol 38 (13): 1–6. PETSOC-99-13-11. https://doi.org/10.2118/99-13-11.
- Tehrani, A., Cliffe, A., Hodder, M. H. et al. 2014. Alternative Drilling Fluid Weighting Agents: A Comprehensive Study on Ilmenite and Hematite. Paper presented at the IADC/SPE Drilling Conference and Exhibition, Fort Worth, Texas, USA, 4–6 March. SPE-167937-MS. https://doi.org/10.2118/167937-MS.
- Tehrani, A., Cliffe, A., Onwuzulike, I. et al. 2011. New Laboratory Technique for Barite Sag Measurements. Paper presented at the Offshore Mediterranean Conference and Exhibition, Ravenna, Italy, 23–25 March. OMC-2011-011.
- Tehrani, A., Zamora, M., and Power, D. 2004. Role of Rheology in Barite Sag in SBM and OBM. Paper presented at the AADE Drilling Fluids Conference, Houston, Texas, USA, 6–7 April. AADE-04-DF-HO-22. https://www.aade.org/application/files/6115/7295/4828/AADE-04-DF-HO-22.pdf.
- Varges, P. R., Costa, C. M., Fonseca, B. S. et al. 2019. Rheological Characterization of Carbopol Dispersions in Water and in Water/Glycerol Solutions. Fluids (15): 3. https://doi.org/10.3390/fluids4010003.
- Yang, H., Kang, W., Yu, Y. et al. 2017. A New Approach to Evaluate the Particle Growth and Sedimentation of Dispersed Polymer Microsphere Profile Control System Based on Multiple Light Scattering. *Powder Technol* 315: 477–485. https://doi.org/10.1016/j.powtec.2017.04.001.
- Zamora, M. 2011. Taming of the Shoe. Paper presented at the AADE National Technical Conference and Exhibition, Houston, Texas, USA, 12–15 April. AADE-11-NTCE-44. https://www.aade.org/application/files/8115/7261/8788/AADE-11-NTCE-44.pdf.
- Zamora, M. and Bell, R. 2004. Improved Wellsite Test for Monitoring Barite Sag. Paper presented at the AADE Drilling Fluids Conference, Houston, Texas, USA, 6–7 April. AADE-04-DF-HO-19. https://www.aade.org/application/files/6315/7295/4830/AADE-04-DF-HO-19.pdf.
- Zamora, M. and Jefferson, D. 1994. Controlling Barite Sag Can Reduce Drilling Problems. Oil & Gas J. 92 (7): 47-52.